Received: 21 July 2020 | Accepted: 12 August 2020

DOI: 10.1111/aae.12167

ORIGINAL ARTICLE

Arabian Archaeology and Epigraphy WILEY

Archaeometric studies on the petroglyphs and rock varnish at Kilwa and Sakaka, northern Saudi Arabia

Meinrat O. Andreae[1,2,3] | **Abdullah Al-Amri**[2] | **Claire M. Andreae**[1] | **Maria Guagnin**[4] | **Klaus Peter Jochum**[1] | **Brigitte Stoll**[1] | **Ulrike Weis**[1]

[1]Max Planck Institute for Chemistry, Mainz, Germany

[2]Department of Geology and Geophysics, King Saud University, Riyadh, Saudi Arabia

[3]Scripps Institution of Oceanography, UCSD, La Jolla, CA, USA

[4]Max Planck Institute for the Science of Human History, Jena, Germany

Correspondence
Meinrat O. Andreae, Max Planck Institute for Chemistry, PO Box 3060, D-55020 Mainz, Germany.
Email: m.andreae@mpic.de

Funding information
Max Planck Society; King Saud University

Abstract

We conducted rock varnish measurements at four rock art sites in north-western Saudi Arabia, including Kilwa and the Camel Site near Sakaka. We determined the areal densities of Mn and Fe in rock varnish that had accumulated on petroglyph surfaces since their creation, complemented by a detailed analysis of varnish samples. We inferred varnish accumulation rates by relating the Mn areal density on inscriptions to their ages estimated based on the type of script used. Applying these rates to the varnish densities on the rock art indicated that the art was produced during two distinct periods, corresponding to the Pre-Pottery/Late Neolithic and the Bronze/Iron Age, respectively, with different artistic traditions, reflecting distinct socioeconomic and ecological conditions. Our dating approach, while admittedly burdened with substantial uncertainties, yields ages consistent with archaeological and historical evidence and it provides a unique quantitative tool to obtain at least rough ages for otherwise undatable rock art.

KEYWORDS

rock art, petroglyphs, rock varnish, manganese, Neolithic, Bronze Age, Iron Age

1 | INTRODUCTION

Rock art, one of the most ancient forms of human artistic expression that has been preserved over the ages since its creation, can give us a window into the minds and lives of our human ancestors. The oldest rock art dates from the Upper Palaeolithic, exemplified by the famous cave paintings in France and Spain, where minimum ages of 41 ka BP (before present) have been documented (Pike et al., 2012), as well as those in the Indonesian archipelago, with minimum ages of 44 ka (Aubert et al., 2019). These images were produced by applying pigments to rock surfaces, creating so-called pictographs, which can be dated either by radiocarbon measurements of the charcoal pigment used or by uranium-series dating of the speleothems that cover the images. Here we focus on another type of rock art: petroglyphs, which are produced by removing dark crusts, so-called rock varnish, from rock surfaces and exposing the lighter coloured host rock underneath.

Petroglyphs are found on all continents inhabited by humans (e.g., Bednarik, 2013, 2014; Francis & Loendorf, 2004; Heizer & Baumhoff, 1962; Khan, 2007; Olsen, 2013; Ramanaidou & Fonteneau, 2019; Soukopova, 2018; Tang et al., 2018; Whitley, 2013; Whitley & Dorn, 2007; Whitley et al., 2017). Because they contain no dateable pigment, they are even more difficult to date than pictographs, and there is thus considerable uncertainty about the age of the oldest

preserved petroglyphs. Ages from the late Pleistocene (*c*.15 ka BP) have been proposed (Bednarik, 2013, 2014; Huyge et al., 2011; Ramanaidou & Fonteneau, 2019; Tang et al., 2018), but petroglyph creation may have begun considerably earlier, considering that they are usually in locations exposed to weathering and thus may only be preserved for some 10–20 ka (Bednarik, 2012). In Saudi Arabia, rock art has been created from around the time of the Neolithic transition until the present, based on an analysis of its content and on archaeometric measurements (Bednarik, 2017; Guagnin et al., 2015, 2016, 2017; Khan, 2007, 2017; Macholdt et al., 2018, 2019).

Several techniques have been applied to the dating of petroglyphs, with varying degree of success. These include radiometric techniques, cation ratio changes, microlaminations, varnish thickness, colorimetric analysis, etc. (Bednarik, 2009, 2010; Cremaschi, 1996; Dorn, 2007; Francis et al., 1993; Liu & Broecker, 2013; Sowers, 2013; Whitley, 2012). Unfortunately, direct dating by classical radiometric techniques has so far rarely been successful (Dragovich, 2000; Watchman, 2000; Zerboni, 2008; Zerboni et al., 2019). In the present study we use an indirect technique to obtain age estimates for petroglyphs, which is based on the fact that, to create a petroglyph, the artist removes the rock varnish and thereby creates a bare host rock surface. Over time, varnish will regrow on this surface until it eventually reaches a coating density more or less identical to its surroundings. The relative degree of varnishing has been used by numerous authors in a qualitative way to visually obtain relative estimate ages (Bednarik, 2009, 2017; Belzoni, 1820; Khan, 2007; Reneau, 1993; Whitley & Dorn, 2007). Quantitative approaches have used colorimetry or measurements of the Mn areal density (i.e., the amount of Mn per unit area) on the petroglyph surface (Bednarik, 2009; Lytle et al., 2008; McNeil, 2010; Reneau, 1993). However, because the rate of varnish growth depends on many variables other than age, including the exposure of the rock surface to dust, erosion by wind and water, orientation and slope of the rock surface, hardness, roughness and texture of the rock underneath, and its initial Fe content, these techniques have to be viewed with caution and the results must be considered as experimental, as discussed in detail by Macholdt et al. (2019).

In several previous studies we developed an improved technique to obtain age estimates from measurements of Mn areal density by portable X-ray fluorescence (pXRF) (Andreae et al., 2020; Macholdt et al., 2018, 2019). In this approach we use the ratio between the Mn density on the petroglyph to that of the surrounding intact varnish as the basis for an age estimate, which corrects for the influence of variables other than age that affect varnish deposition. The varnish growth rates are calibrated by measuring on petroglyphs for which independent age estimates are available, such as particular types of scripts that had been used during specific time periods, or images of animal species that represent dated paleoclimatic transitions (Guagnin et al., 2015, 2016; Robin, 2018; Robin & Gorea, 2016; Stein, 2013). In these studies, we found relatively similar rates of varnish regrowth and could demonstrate that the age estimates so obtained were consistent with ages based on the cultural and ecological content of the rock art, and allowed a meaningful ordering of rock images into an age sequence. Given the scarcity of alternative dating methods, especially those that do not require destructive sampling, even the relatively rough age estimates we obtained in this way are a valuable contribution to the archaeological study of rock art.

For the present study, we aimed to extend the geographical, cultural and climatic range of our previous work. The study sites at Kilwa and Sakaka are in northernmost Saudi Arabia (Fig. 1) and are under the influence of a Mediterranean climate with a rainy season peaking in January, in contrast to the Hima region, which is influenced by the Indian Ocean Monsoon. Sakaka receives about 60 mm rainfall per year, about half the amount of our previous study sites in Saudi Arabia. While the cultural influences in the Hima region were dominated by the interactions with the region to the south, including Yemen, Hadramaut, Sanaa and Asir, the present study area lies north of the Nafud Desert, with major river drainages connecting it to the Levant and Mesopotamia (Magee, 2014a). This makes this region the interface between the cultures of the Arabian Peninsula and the Fertile Crescent to the north (Fujii, 2013; Zarins, 1990). Sakaka and Hima both lie on a major caravan trading routes, whereas Kilwa is in a fairly remote region with no major trade routes nearby.

The petroglyphs are produced by removing the dark rock varnish that coats much of the rock surfaces in the study area. Rock varnish is a thin, dark, Mn-rich coating found in a variety of environments worldwide (Dorn, 2007; Engel & Sharp, 1958; Krinsley et al., 2013; Liu & Broecker, 2013; Macholdt et al., 2017b, *passim*). It consists of a matrix of poorly crystallised Mn and Fe oxides and hydroxides (oxyhydroxides) in which clay and other detrital minerals are embedded (Bishop et al., 2002; Dorn, 2007; Dorn et al., 2013; Potter & Rossman, 1977, 1979). The varnish in the study area is classified as a type I varnish, which prevails in arid regions and is generally characterised by a layered structure, high rare earth element (REE) and Ba enrichments, and birnessite as the dominant Mn mineral (Macholdt et al., 2017b). While there is an ongoing debate about the details of rock varnish formation, there is now a broad consensus that the Mn and other enriched elements in the varnish matrix, as well as the embedded detrital minerals, are derived from dust deposition and are transformed into the varnish coating by a sequence of dissolution and re-precipitation events (e.g., Dorn & Krinsley, 2011; Goldsmith et al., 2014; Perry et al., 2005; Thiagarajan & Lee, 2004; Xu et al., 2019). For further details and references on this issue, see Andreae et al. (2020), Macholdt et al. (2017b, 2019) and Otter et al. (2020).

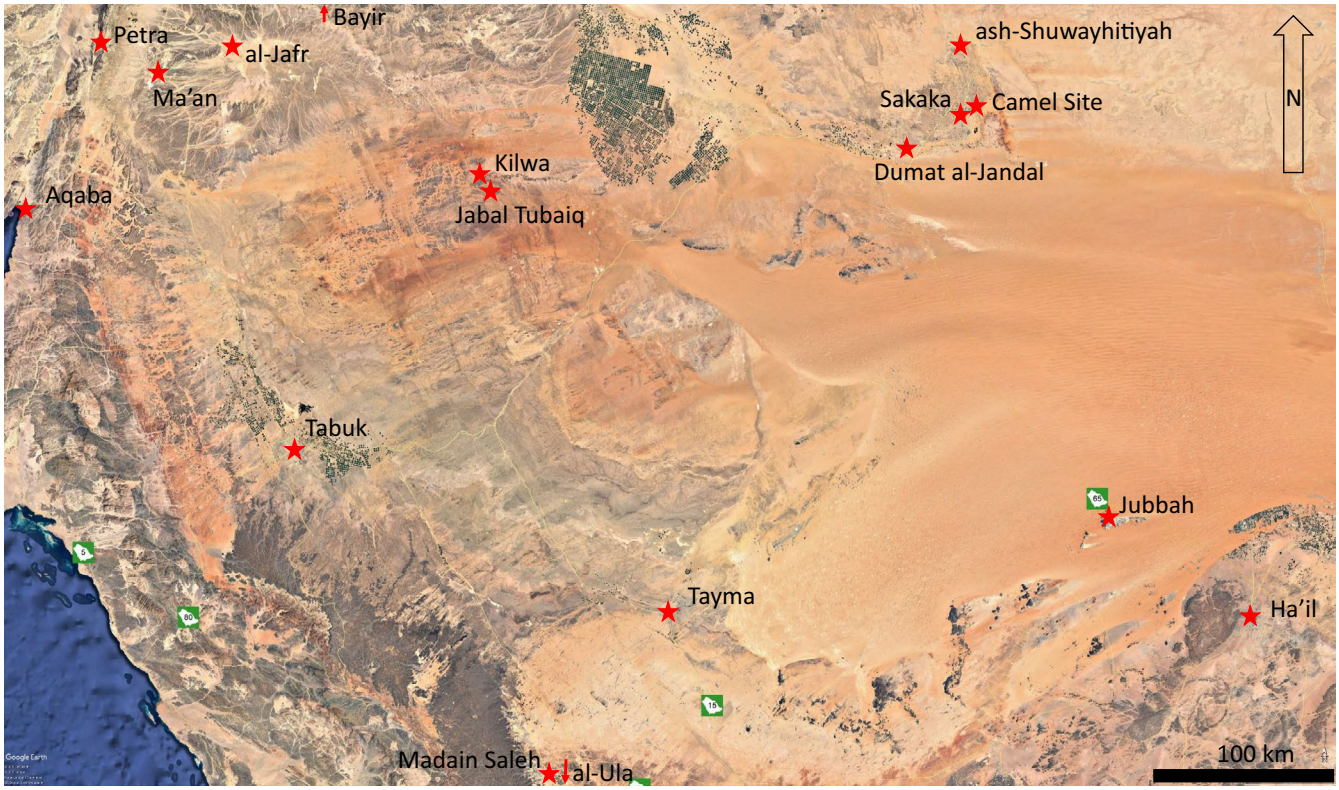

FIGURE 1 Overview map of the study region and related places in north-western Arabia. Courtesy: Google Earth

In spite of the widespread occurrence of rock varnish and the large numbers of publications discussing various aspects of its geochemistry, there is still very little quantitative information on its rate of formation in different geological and climatic settings. The available data show that it develops exceedingly slowly, on the order of micrometres per thousand years (Liu & Broecker, 2000). In the present study, we have focused on the rate of Mn and Fe accumulation in the varnish, which can be more easily quantified in a representative fashion by making numerous measurements of the Mn and Fe areal densities using pXRF (Andreae et al., 2020; Macholdt et al., 2018, 2019; McNeil, 2010; Reneau, 1993). In the present study, we extend the range of available data to the most arid region studied by our approach so far. We complement these geochemical aspects of this study by major and trace element analyses of the varnish to investigate the trace element enrichments in the varnish and compare them with results from other regions.

Here we present the results from *in-situ* measurements by pXRF on intact rock varnish, petroglyphs and inscriptions from two areas in northernmost Saudi Arabia, from which we determine the areal density, D_{Mn} and D_{Fe}, of Mn and Fe. Using palaeographic age estimates of some inscriptions as calibration points, we derive estimates of the rate of varnish regrowth on the rock art. We then use these regrowth rates to estimate the age of petroglyphs of unknown age, and examine these results in the cultural and palaeoecological context reflected in the rock art.

2 | BACKGROUND: STUDY REGION, CLIMATE AND HISTORY

The study region is located in northernmost Saudi Arabia and comprises two main sites (Fig. 1). The Camel Site (30.0227°N, 40.2876°E, 569 masl) is located about 10 km north-east of the city of Sakaka, while the Kilwa Site (29.7023°N, 37.5482°E, 1020 masl) is at a remote location in the Jabal Tubaiq hills. In addition, a few measurements were made at Hudrah Cave (29.9908ºN, 40.1987°E, 556 masl), a small rock shelter near the ancient well Bi'r Saisara in Sakaka, and on a hilltop site in Jabal Tubaiq along the track to Kilwa (29.6092°N, 37.5908°E, 896 masl).

The region has a Mediterranean desert climate, in the class BWh (arid desert, low latitude) of the Köppen–Geiger classification. The average annual temperature at al-Jawf/Sakaka airport is 22.6°C, with an average high of 40.7°C in July and an average low of 3.9°C in January. Average annual precipitation is about 60 mm, with a winter rainy season peaking in January (www.weather-atlas.com/en/saudi-arabia/sakaka-climate).

During the late Pleistocene and Holocene, Arabia underwent large oscillations in wetness, with extreme aridity during the last glacial maximum (LGM) until *c*.12 to 10 ka BP, followed by the Arabian Humid Period (AHP) lasting from *c*.10 ka to *c*.5–6 ka BP (Engel et al., 2012; Lezine et al., 2007; Magee, 2014a; Parker, 2010). A dry climate, resembling the

present-day arid conditions, established itself after the end of the AHP, interspersed with occasional more humid episodes (Garrard & Harvey, 1977; McClure, 1976; Parker, 2010).

Evidence for hominin occupation in the study region goes back to at least the Middle Pleistocene, as shown by Lower Palaeolithic (Acheulean and possibly Oldowan) tool assemblages found at ash-Shuwayhitiyah, 40 km north of Sakaka (Petraglia, 2003), and similar assemblages at Kilwa itself (Gilmore et al., 1982; Rhotert et al., 1938). The Middle Palaeolithic is represented at Kilwa by a large number of Mousterian and Levallois tools (Gilmore et al., 1982; Rhotert et al., 1938). It is unclear whether hominin presence continued into the Upper Palaeolithic (40 to 10 ka BP), as no artefacts from this period have been found in the region (lnizan, 2012). This may have been due to the cold and extremely dry climate during the LGM, making a hunting–gathering lifestyle unfeasible (Uerpmann et al., 2010).

With the warming and moister climate at the beginning of the Holocene *c*.12 to 10 ka BP, human presence in Arabia resumed during the AHP in the form of hunter–gatherers and later nomadic pastoralists with domestic cattle, sheep and goats (Guagnin et al., 2016, 2017; Magee, 2014b; Zarins, 1990). Hunted species include ibex, wild goat, oryx, gazelle, kudu, aurochs, dromedary, wild ass, boar and ostrich (Guagnin et al., 2016, 2018b; Munro et al., 2018). Pastoralists may have moved in from the Levant and thus arrived fairly early in north-western Arabia (Magee, 2014b). The moist climate during the AHP also allowed the existence of the wild bovid species, aurochs (*Bos primigenus*), which requires access to water every few days, as well as the development of cattle herding *c*.8500 BP (Drechsler, 2007; Guagnin et al., 2016; McCorriston & Martin, 2010; Uerpmann, 2002; Uerpmann et al., 2010). The Neolithic in north-western Arabia has not been archaeologically explored in great detail, and therefore the chronology of Neolithic occupation is relatively vague. The survey of the Northern and Northwestern Regions in 1980–81 identified several Pre-Pottery Neolithic (PPN) sites in this region, including Kilwa, but provides little detail (Gilmore et al., 1982; Ingraham et al., 1981). However, detailed work just across the border in Jordan suggests the development of a mixed economy, including pastoral transhumance, hunting and small-scale agriculture in the Pre-Pottery Neolithic B (PPNB) *c*.10 to 8 ka BP, shifting towards pastoral nomadism in the Late Neolithic (LN) after *c*.8 ka BP (Betts, 1987; Fujii, 2013). With the climate-driven shift from grasslands to shrublands, cattle herding became increasingly less viable after *c*.7000 BP and disappeared *c*.6000 BP (Dinies et al., 2015; Guagnin et al., 2016; Lezine et al., 2007). At Kilwa, Neolithic human activity is evident from the presence of a huge number of microlithic blades (Gilmore et al., 1982; Rhotert et al., 1938), which are found in direct proximity to the main concentration of rock art. Based on archaeological and thematic considerations, Zarins (1990) associated the early rock art at Kilwa with the PPNB. Human activity in the region during the Chalcolithic is evident from finds of pottery, stone circles and, most spectacularly, the assembly of large standing stone slabs at Rajajil, about 10 km south of Sakaka, dated to *c*.6–7 ka BP (Almushawh, 2018; Gebel, 2016; Hashim, 1996; Zarins, 1979).

When arid conditions returned at the end of the AHP, *c*.5–6 ka BP, a decline in human populations and a shift in subsistence strategies towards sedentary horticulture or coastal resources is reflected in both the archaeological record (Gebel, 2016; Hoyland, 2001; Magee, 2014b; Uerpmann, 2002) and a dearth of rock art creation (Khan, 2007). In the Bronze Age, human activity in north-western Arabia included irrigation agriculture beginning *c*.4000 BP, as shown by the construction of the walled city of Tayma with its associated hydraulic structures (Klasen et al., 2011; Magee, 2014a). Rock art from this period includes humans wearing lunate pommel-handled daggers as diagnostic feature (Newton & Zarins, 2000). Around the same time, the hunting of wild dromedaries intensified, possibly as a response to the diminishing supply of pastoral species due to increasing aridity (Magee, 2014a; Uerpmann & Uerpmann, 2012).

The earliest morphological evidence for the domestication of the dromedary camel has been dated to *c*.3000 BP, around the Bronze/Iron Age transition (Uerpmann & Uerpmann, 2012). This enabled substantial socioeconomic changes because it made possible both a herding economy based on an arid-adapted animal and facilitated long-distance trade from southernmost Arabia to the Levant and Mesopotamia (Hoyland, 2001; Magee, 2014a; Uerpmann & Uerpmann, 2012). The Midianites, some of whom were specialised camel herders, likely ruled the Tabuk region *c*.3000 BP, trading south as far as Yemen (Ingraham et al., 1981; Potts, 2012; Robin & Al-Ghabbān, 2017). Qurayyat, which lies on the route from Adumatu (as today's Dumat al-Jandal, Al-Jawf, was called at that time) to the Levant, was one of their main centres (al-Ghazzi, 2012).

As a consequence of increasing trade, the oases of northern Arabia, including Tayma and Adumatu, become closely tied to Mesopotamia. In 691 BCE, Sennacherib, ruler of Assyria, pursued an Arabian army to Adumatu and captured thousands of camels. His son, Essarhaddon, restored cult statues to Adumatu in 678 BCE, and received camels as tribute. Sennacherib's grandson, Assurbanipal, crushed several rebellions by Arabian tribes in the years following 649 BCE. Later, Nabonidus of Babylon led an army to Tayma and stayed there from 553 to 543 BCE (Potts, 2012). Towards the end of the first millennium BCE, writing developed in northern Arabia, using several variants of the Ancient North Arabian (ANA) script, which in the present study region include Safaitic, Dumaitic, Hismaic and Mixed Safaitic–Hismaic (MSH) (Hoyland, 2001; Macdonald, 2000, 2010; Norris, 2018).

The Nabateans, who were originally nomadic Arabs, came to dominate the caravan trade in northern Arabia *c*.300–200 BCE (Bowersock, 1994; Hoyland, 2001; Wenning, 2007). They also introduced their own script, Aramaic, which replaced the ANA scripts by the first century CE in the oases, while the nomads continued to use ANA scripts until the fourth century CE (Macdonald, 2010). The Nabateans were established at Petra in the third century BCE, and their kingdom extended at least as far south as Hegra (Ḥigrâ', al-Hijr, modern Mada'in Salih) (Nehmé et al., 2006, 2012, 2014). One of their trade routes passed through Dumat al-Jandal and Sakaka, connecting Hegra and Tayma to Mesopotamia (Charloux, 2018; Charloux & Loreto, 2011). The Kilwa site lies near two minor camel trails and desert tracks, one connecting Aqaba and Petra to Dumat al-Jandal via Maʿan, El Jafr and Wadi Sirhan, the other Amman to Tayma via the Bayir Wells. These tracks might also date to the Nabatean period; they still existed in the early twentieth century and were used by Gertrude Bell (Bell, 1927), Agnes and George Horsfield (Horsfield, 1943; Horsfield et al., 1933), and Hans Rhotert's team (Rhotert et al., 1938). The Nabateans' regime ended abruptly in 106 CE by the Roman annexation, and Dumat al-Jandal became part of Arabia Petraea (Charloux & Loreto, 2013).

The early part of the first millennium CE, before the arrival of Islam, saw a strong Christian influence, with several Bedouin tribes converting to Christianity (Gilmore et al., 1982). This period is represented at Kilwa by the remains of monastic cells and cross symbols at several locations at the site (Bell, 1927; Horsfield, 1943; Horsfield et al., 1933; Rhotert et al., 1938). Islam was established at Dumat al-Jandal beginning in 626 CE by raids led by Prophet Muhammad and consolidated *c*.634 CE under first caliph Abu Bakr (Charloux & Loreto, 2013). Christianity appears to have coexisted with Islam in northern Arabia for some time (Hoyland, 2017).

While Dumat al-Jandal had been visited by numerous European travellers and explorers during the nineteenth and early twentieth centuries (Charloux & Loreto, 2013), the first European to reach Kilwa was the British explorer/politician/diplomat Gertrude Bell, who made a brief side trip to Kilwa on her way from Amman across the Nafud to Ha'il in February 1914 and recorded:

> the ruin was worth seeing. It has a Kufic graffito and all complete and to get to it I rode five hours across the Jebel Tubaiq, saw and photographed a pre-Muhammadan High Place (so I take it to be) and got a far better idea of these exceedingly interesting hills. (Bell, 1927)

In the two hours Bell spent at Kilwa, she saw and photographed only the ruins of the early Christian monastery, and the discovery of the rock art had to await the expedition of the Horsfields and Nelson Glueck in 1932 (Horsfield, 1943; Horsfield et al., 1933). As they had run out of water, they could only stay half an hour at Kilwa, but managed to photograph several of the petroglyphs, including those of an aurochs, a wounded ibex and some human figures (Horsfield et al., 1933).

The work of the Horsfields and Glueck inspired Rhotert's German expedition to Kilwa in 1934, which spent six weeks in Kilwa, collecting and cataloguing lithic material (over 5000 items), mapping the site, and photographing and sketching a large part of the rock art. They found a clear association between the rock art their central site, which they named 'Horsfieldberg', and a large number of PPN lithics scattered around the base of this hill. In this study we focus our measurements on the rock art elements included in the monograph based on this expedition (Rhotert et al., 1938).

Kilwa was visited briefly (two days) by archaeologists of the Saudi Arabian Comprehensive Archaeological Survey Program in 1981, who collected and described lithics and surveyed the monastic cells, largely confirming the work of the Rhotert group (Gilmore et al., 1982). Work at Kilwa by a French–Saudi team began in 2008 and included excavations in the monastery area as well as archaeological and epigraphic surveys in the surroundings (Farès, 2010, 2011). They suggested that the monastery was constructed by Syrian Christians, probably before the eighth century CE (Farès, 2010).

A large amount of work was carried out in the Sakaka–Dumat al-Jandal area starting in 2009 by the Saudi–Italian–French Archaeological Project, with important finds spanning the Palaeolithic to the Nabatean periods (Charloux, 2018; Charloux & Loreto, 2011, 2013; Loreto & Charloux, 2013), including the discovery of the Camel Site (Charloux et al., 2018). This project included an epigraphic survey of the region, which yielded a large number of ANA (Safaitic, Hismaic, MSH, etc.), Nabatean and early Arabic inscriptions (Nehmé, 2017).

3 | METHODS AND MATERIALS

3.1 | Site descriptions

3.1.1 | Camel Site (Sakaka)

The Camel Site (CS; 30.0227°N, 40.2876°E, 570 masl) consists of a group of small sandstone spurs of the Wasia Group located about 8 km north-east of Sakaka (Charloux et al., 2018). On the faces of these spurs are low-relief engravings of near-life-size dromedaries and equids. Many of these are heavily eroded, but there are still fragments in

a good state of preservation with heavy coatings of rock varnish. Some of the cliff faces also contain two-dimensional petroglyphs and inscriptions in ANA scripts and Arabic. About 650 m north-north-east of CS (30.0288°N, 40.2896°E) is a group of small outcrops with petroglyphs and ANA writing, where we made additional measurements on an MSH inscription. Varnish sample SAK03 was collected at CS from the top of the hill at 30.02284°N, 40.02874°E.

3.1.2 | Hudrah Cave (Sakaka)

Hudrah 'Cave' (HC; 29.9908°N, 40.1987°E) is a small rock shelter under a prominent overhang, 130 m south-south-east of Bi'r Saisara well (likely of Nabatean age). The front ledge of the overhang contains some petroglyphs and Arabic writing on which a few measurements were made.

3.1.3 | Kilwa

The Kilwa site consists of a few small inselbergs located adjacent to the ruins of a monastery (details of its history are presented above). The largest number of petroglyphs is found on a hill, which Rhotert named 'Horsfieldberg' (HFB, 29.7023°N, 37.5482°E, 1020 masl) in honour of the Horsfields, who had provided the first description of the rock art at this site. About 400 m north-west of the HFB is a smaller inselberg, named 'Kleiner Horsfieldberg' (KHB; 29.7053°N, 37.5463°E), which has numerous petroglyphs of younger ages, as suggested by Rhotert et al. (1938) based on the thin rock varnish found on the rock art there. Another inselberg, 'Altarberg' (AB, 29.6974°N, 37.5475 E°) lies 530 m south of HFB. The rock art here consists predominantly of crosses that are likely related to the monastery, which lies *c*.650 m north-west of it. Given the high level of disturbance in the monastery site, we only made a few measurements there, which included the lintel that had first been mentioned by Bell. Varnish samples KIL02 and KIL03 were collected at KHB (29.70522°N, 37.54632°E) and HFB (29.70208°N, 37.54830°E), respectively.

3.1.4 | Jabal Tubaiq hill

Our guide pointed out a hill along the track to Kilwa in the Jabal Tubaiq mountains, which had several inscriptions and petroglyphs around its top (Jabal Tubaiq (JT); 29.6092°N, 37.5908°E). The inscriptions are in Hismaic script, and the most common rock art elements represent camels. This site has not been reported on previously in the literature.

3.2 | Methods

3.2.1 | Portable X-ray fluorescence spectrometry

The pXRF measurements were conducted in the same way as in our previous studies, where they are described in detail (Macholdt et al., 2018, 2019), and will only be outlined here briefly. Measurements were conducted using a Niton XL3 pXRF (Thermo Fisher Scientific) in 'mining' mode. The filter steps and integration periods were: 'standard' 25 s, 'low' 15 s, 'high' 20 s and 'light' 25 s. The instrument was equipped with an X-ray source with an energy of 50 keV and a silver anode, and had a spot size of 8 mm in diameter. For quality control, the reference materials TILL-1 and FeMnOx-1 (GeoReM database, v.25; http://georem.mpch-mainz.gwdg.de) (Jochum et al., 2005) were measured before and after each X-ray fluorescence (XRF) measurement sequence. We made a total of 894 measurements, 358 on intact varnish surfaces, 473 on petroglyphs and the rest for ancillary purposes, for example, on freshly exposed bare sandstone substrate and standards.

Whereas the measurement results from the bare sandstone are valid as provided by the pXRF software in mass concentration units, the measurements on the rock varnishes had to be converted into areal densities, D_{Mn} (μg cm^{-2}), using the calibration curve from Macholdt et al. (2017a). To correct for the underlying sandstone contribution, the Mn and Fe concentrations of the unvarnished sandstone were determined by conducting measurements on nearby freshly exposed rock surfaces, and these values were subtracted from those measured on the varnished surfaces. For Mn, the background values were always at or below the detection limit, whereas for Fe they were significant and highly variable, with a mean and standard deviation (SD) of 124 ± 110 μg cm^{-2}. The areal density of Fe (D_{Fe}) was calculated using the Mn calibration values and the Mn/Fe sensitivity ratio, and is thus subject to a greater uncertainty (estimated at about 20%). Since D_{Mn} and D_{Fe} vary substantially due to different growth and erosion conditions, even within each rock art panel location, we also calculated the ratio of the measurements on the petroglyph surfaces to that on immediately adjacent intact varnish. This provides a normalised measure, called N_{Mn} and N_{Fe} (%), which basically expresses the degree of revarnishing on the petroglyph surface relative to the surrounding intact varnish. The measurement and data-reduction techniques used were identical to those in Macholdt et al. (2018) and are described in more detail there. Photographs of all petroglyph measurement locations are provided in the additional supporting information.

3.2.2 | Femtosecond LA-ICP-MS

The femtosecond laser ablation inductively coupled plasma mass spectrometry (fs-LA-ICP-MS) measurements were carried out using a ThermoFisher Element 2 single-collector sector-field ICP-mass spectrometer combined with a 200 nm fs-LA system, NWRFemto (Elemental Scientific Inc.). LA was conducted in a new wave large format cell using a He atmosphere. Subsequent to the ablation, the He carrier gas was mixed with an Ar gas flow to transport the aerosols generated by ablation to the ICP-MS. All measurements were conducted in medium mass resolution mode (2000) with flat-top peaks. Two scan modes were used: surface scans with the laser scanning along the surface of the varnish, and profile scans on sections cut through the rock, providing a cross-section of the varnish. The rock varnish measurements were executed as *in-situ* line scans, after pre-ablation with an 80 µm s^{-1} scan speed and spot size of 65 µm. The operating parameters of the laser system during the measurements were: for the surface scans, spot size: 55 µm, pulse repetition rate: 50 Hz, energy density: about 0.1 J cm^{-2}, scan speed: 2 µm s^{-1}; for the profile scans, spot size: 40 µm, pulse repetition rate: 50 Hz, energy density: about 0.1 J cm^{-2}, scan speed: 1 µm s^{-1}. Blank measurement time was 15 s and washout time was 30 s. The analytical error of the measurements is of the order of 2–6% for the elements measured. Measurements with MnO_2 mass fractions of < 2% were rejected as contamination from the underlying rock material. The reference glass GSE-1G (GeoReM database) was used for calibration. To normalise the data, the oxides of the major elements (Na_2O, MgO, Al_2O_3, SiO_2, P_2O_5, K_2O, CaO, TiO_2, MnO_2, and Fe_2O_3) were assumed to add up to 98 mass%.

3.2.3 | Data analysis

Regression calculations were made using bivariate regression, which takes into account error in both the *x* and *y* variables, using the Williamson–York iterative bivariate-fit algorithm (Cantrell, 2008).

4 | RESULTS AND DISCUSSION

4.1 | Rock varnish chemical composition

We analysed three varnish samples (one from CS, SAK03, and two from Kilwa, KIL02 and KIL03) by fs-LA-ICP-MS for their major and trace element composition. The results will be only discussed briefly here, since a separate paper with a detailed discussion of the geochemistry of the varnish and the associated aeolian dust is in preparation.

The composition of the varnish is typical of type I rock varnish from arid regions, with Mn, Fe, Si and Al as the most abundant elements, present in the form of Mn-Fe oxyhydroxides, clay minerals and quartz grains (Dorn, 2007; Macholdt et al., 2017b; Potter & Rossman, 1977). The average mass percentages of Mn in the varnish and their SDs are 2.9% ± 1.4% and 6.5% ± 3.7% in CS and Kilwa samples, respectively; the corresponding values for Fe are 4.8% ± 1.8% and 7.9% ± 3.3%. The average mass ratios of Mn to Fe measured by fs-LA-ICP-MS are 0.60 ± 0.38 at CS and 0.82 ± 0.58 at CS and Kilwa, in good agreement with the average of 0.85 ± 0.62 obtained by the pXRF measurements discussed below. The relatively low Mn concentrations and Mn/Fe ratios are consistent with varnish development under predominantly arid conditions (Liu & Broecker, 2008; Liu et al., 2000; Macholdt et al., 2017b).

Figure 2 shows the elemental composition data in the form of enrichment factors against the average upper continental crust composition (Rudnick & Gao, 2003). For comparison, Figure 2 also shows statistics of the results of our previous measurements on type I varnish. The enrichment patterns in CS and Kilwa samples are in good agreement with published

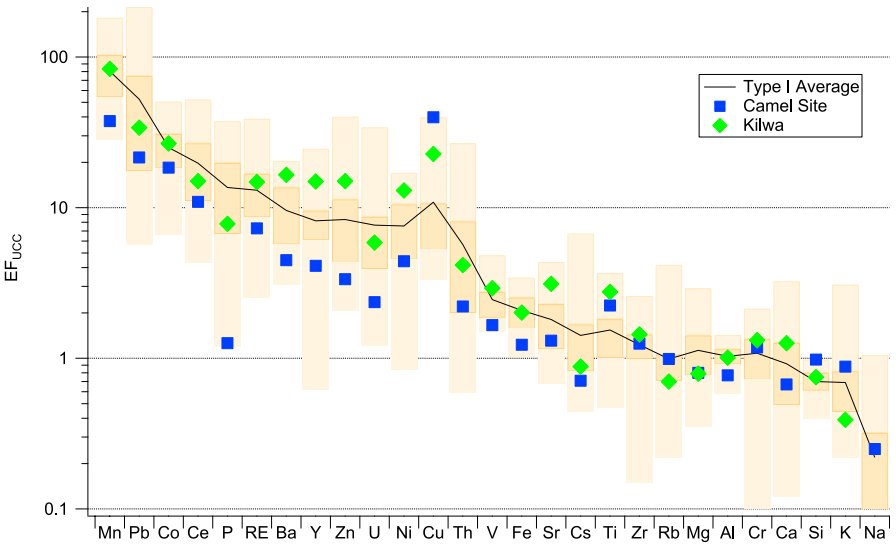

FIGURE 2 Chemical composition of the rock varnish from the Camel and Kilwa sites expressed as enrichment factors versus average upper continental crust. (RE, sum of rare earth elements, including Ce and Y)

values for the elements typically enriched in varnish, for example, Mn, Pb, Ba, Co and Ce (Andreae et al., 2020; Dorn, 2007; Macholdt et al., 2017b; Otter et al., 2020; Potter & Rossman, 1977; Xu et al., 2019).

There is a systematic difference between the enrichment patterns of the CS and Kilwa samples, with the Kilwa sample showing much higher enrichment in the typical varnish elements, while the CS sample is less depleted in the crustal elements, for example, Na, K, Si and Al, suggesting that the CS varnish contains less Mn/Fe oxyhydroxides and more residual quartz grains and clay minerals. A high Ti content indicates the presence of residual rutile grains, whereas the low Ca content suggests a low abundance of Ca carbonate and/or smectite clay minerals. Both sites have unusually high Cu enrichments, with CS showing the highest EF_{Cu} in our entire data set of type I varnishes from arid sites worldwide. This may be related to the presence of numerous copper mining and smelting sites in the Arabah Valley region, upwind from the study region, where mining and smelting activity has been documented from the LN (7000 BP) to medieval Islamic times (*c*.1400 CE) (Grattan et al., 2016; Hauptmann, 2007). Widespread pollution in soils and riverbeds has been found in the region (Beherec et al., 2016; Grattan et al., 2016) and may have been transported to the study sites by aeolian dust. In contrast, Pb enrichments at the sites are relatively low compared with our previous work. This may be related to the low levels of automotive Pb in this remote region, in contrast to some of our previous sites, especially those in the Mojave Desert of California (Andreae et al., 2020).

4.2 | Areal density of Mn and Fe in the rock varnish

Figure 3a presents the results of the pXRF measurements on intact rock varnish from all sites in the form of a scatter plot of the areal densities, D_{Mn} versus D_{Fe}; the corresponding statistics are given in Table 1. The averages from the four sites are shown as larger symbols with error bars representing the variability of the varnish covers on the different measurement spots. The large variability of the areal density reflects the well-known fact that the density of rock varnish coatings is dependent on a large number of factors, including rainfall, dust fall, slope angle, substrate durability, surface runoff, etc. (for a detailed discussion, see Macholdt et al., 2019).

The D_{Mn} averages from all sites fall very closely to each other and are not significantly different, so that an overall D_{Mn} average of 209 ± 78 μg cm^{-2} appears to be representative of rock varnish coatings in the study area. This value is significantly higher than the results from our previous measurements in Arabia, with 105 ± 55 μg cm^{-2} in the Hima region (Macholdt et al., 2018) and 156 ± 94 μg cm^{-2} in the Ha'il region (Macholdt et al., 2019). The potential reasons for this difference include differences in age, dust availability, rock substrate, rainfall and others. There is not enough detailed information about dust fluxes in Arabia to draw firm conclusions, but available models suggest similar dust fluxes for the three regions in the Pleistocene and Holocene (Bergametti & Forêt, 2014; Jickells et al., 2005; Sudarchikova et al., 2015), making differences in dust flux an unlikely explanation. While differences in rainfall may play a role, as Broecker and Liu (2001) have shown a weak positive relationship between rainfall and Mn content of rock varnish, our measurements actually show the opposite trend, with higher Mn values at our northern sites in spite of lower rainfall here (about 60 mm annually) than at Ha'il and Hima (about 170 and 130 mm annually, respectively). In our study in California, we proposed the much larger weathering resistance of the basalt substrate as a reason for the high Mn densities found there (average of 550 ± 290 μg cm^{-2}) (Andreae et al., 2020). While all three Arabian study regions have sandstone as a rock substrate, it is possible that a somewhat more weathering-resistant sandstone at our present sites may help explain the higher D_{Mn} there.

With the exception of the measurements at the HC site, the mean D_{Fe} at our sites is also very similar (Fig. 3a). The mean D_{Fe} for all sites is 246 ± 153 μg cm^{-2}, comparable with the values from our previous studies (330 ± 80 μg cm^{-2} at Hima and 185 ± 121 μg cm^{-2} at Ha'il). The D_{Fe} values from HC are lower than the average results from the other sites, but still well within the range of variability from the other sites, and thus the low average from HC might just be an artefact of the small number of measurements made there.

The overall mean Mn/Fe ratio in the intact varnishes is 0.85 ± 0.62, close to that from Ha'il (0.91 ± 0.64), but much higher than that from Hima (0.32 ± 0.16). They fall well within the range of Holocene varnishes from a wide range of sites, which typically have Mn/Fe values in the range of 0.22–1.30 (Goldsmith, 2011; Lebedeva et al., 2019; Macholdt et al., 2018, 2019; Thiagarajan & Lee, 2004; Wayne et al., 2006). Like at our previous sites, we find a moderate, but highly significant correlation between D_{Mn} and D_{Fe} in the varnish, with a slope and intercept of 0.33 ± 0.02 and 127 ± 7 ($N = 358$; $r^2 = 0.29$; coefficients given with standard error, SE).

The D_{Mn} and D_{Fe} results from the measurements inside the petroglyphs are shown in Figure 3b; the corresponding statistics are given in Table 1; and the data from individual rock art elements are shown in Table 2. The values span the same range as those for the intact varnish, suggesting a great age of some of the rock art, but the average areal densities are lower, as would be expected for a mixture of varnishes spanning a wide range of ages. The lowest D_{Mn} averages are found at the HC and JT sites, consistent with their younger ages suggested by the Hismaic and Arabic writing found

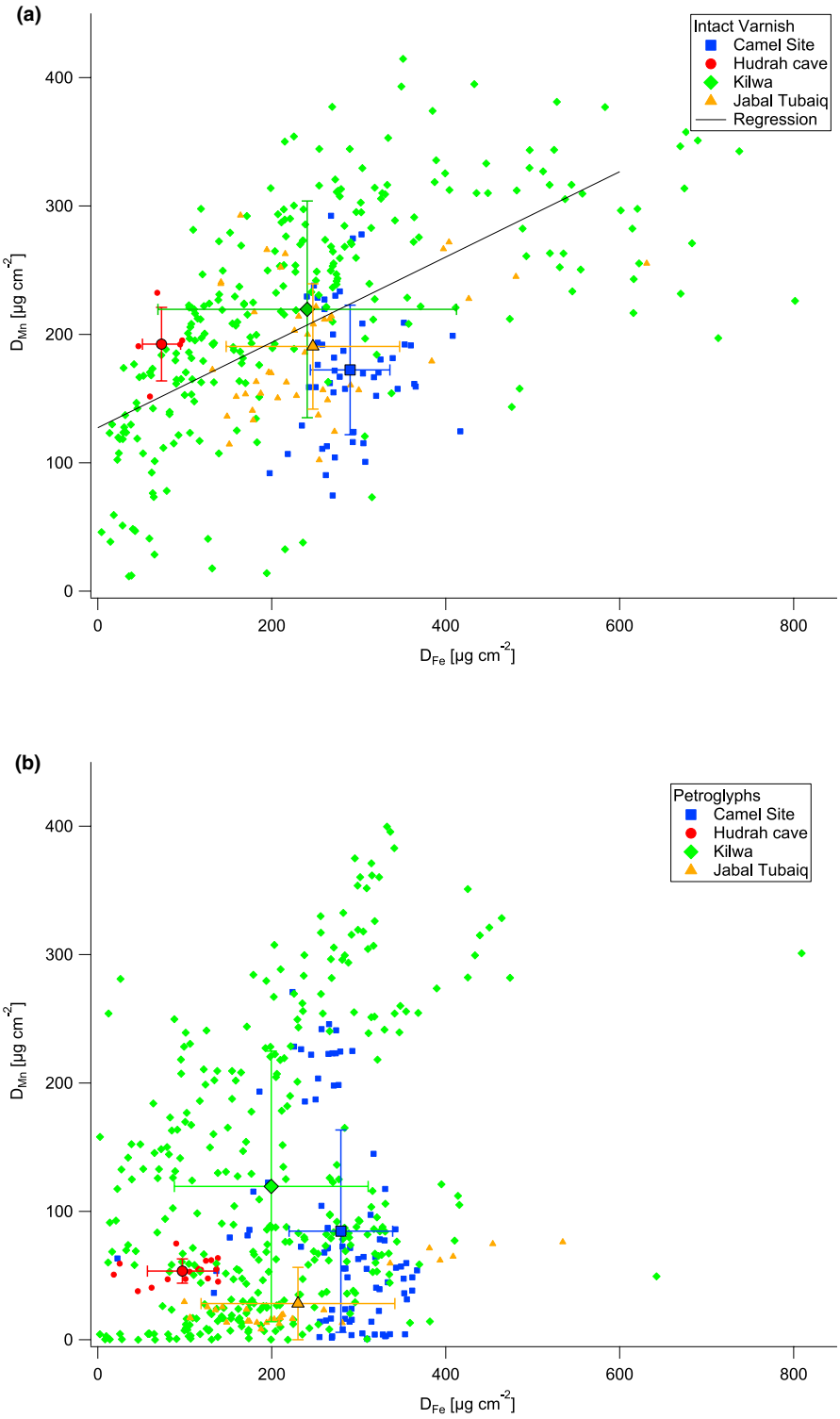

FIGURE 3 Areal density of Mn (D_{Mn}) versus areal density of Fe (D_{Fe}) on rock varnishes in the study area: (a) intact rock varnish and (b) petroglyphs and inscriptions

there. The D_{Mn} at the CS and Kilwa sites span similar ranges and have similar averages, suggesting that they may cover similar creation periods. The average Mn/Fe ratios on the petroglyphs are lower than on the intact varnish, which may be related to the fact that part of them were created after the onset of the extremely arid conditions, when the Mn concentration in the varnish is expected to be lower (Liu & Broecker, 2008; Liu et al., 2000).

4.3 | Normalised areal density of Mn and Fe on the petroglyph surfaces

Figure 3b highlights the large variability of varnish areal density on the rock art elements, which in addition to the exposure age of the petroglyph surfaces is strongly dependent on a large number of variables, particularly surface moisture, inclination, water runoff over the rock surface, weathering resistance

TABLE 1 Mn and Fe areal density, normalised areal density, and Mn/Fe ratios from portable X-ray fluorescence (pXRF) measurements on rock varnish

Site	*N*	D_{Mn} (μg cm^{-2})			D_{Fe} (μg cm^{-2})			Mn/Fe ratio	
		Avg	SD	CV (%)	Avg	SD	CV (%)	Avg	SD
Intact varnish									
Camel Site	50	172	50	29%	290	46	16%	0.60	0.20
Hudrah Cave	5	192	29	15%	73	22	30%	2.81	0.94
Kilwa	260	218	85	38%	239	172	71%	0.91	0.74
Jabal Tubaiq	43	191	49	26%	247	100	40%	0.77	0.37
All intact varnishes	358	209	78	37%	246	153	62%	0.85	0.62
Petroglyphs									
Camel Site	83	85	79	93%	279	60	21%	0.30	0.29
Hudrah Cave	16	54	10	18%	97	40	41%	0.55	0.25
Kilwa	336	119	105	88%	199	111	56%	0.60	0.63
Jabal Tubaiq	29	28	21	76%	230	110	48%	0.12	0.11
All petroglyphs	473	107	100	94%	213	108	51%	0.50	0.53
Normalised densities on petroglyphs									
	N	N_{Mn} (μg cm^{-2})			N_{Fe} (μg cm^{-2})				
		Avg	SD	CV (%)	Avg	SD	CV (%)		
Individual spots									
Camel Site	27	41	32	78%	99	17	17%		
Hudrah Cave	4	28	2.4	9%	138	31	22%		
Kilwa	136	54	41	76%	103	61	59%		
Jabal Tubaiq	12	17	11	68%	94	34	36%		
All petroglyphs	179	49	40	80%	102	55	53%		
Element averages									
Camel Site	9	31	31	102%	102	14	14%		
Hudrah Cave	1	28	–	–	138	–	–		
Kilwa	38	51	41	80%	103	56	55%		
Jabal Tubaiq	3	19	12	65%	98	31	32%		
All petroglyphs	51	45	39	86%	101	49	49%		

Note: Avg, arithmetic average; SD, standard deviation; CV, coefficient of variation.

of the rock substrate, dust deposition flux, etc. (Macholdt et al., 2019, *passim*). To reduce the influence of these factors, we introduced the normalised areal density, N_{Mn} or N_{Fe}, as a metric for the degree of varnish regrowth on a petroglyph surface after removal of the original varnish by pecking or abrasion to create the petroglyph (Macholdt et al., 2018). N_{Mn} or N_{Fe} (%) are defined as the areal density of Mn or Fe on a petroglyph surface divided by that on an adjacent intact rock varnish surface. They can be understood as the percentage of varnish regrowth on the rock art surface since its creation, and since the measurements on the rock art and the adjacent intact varnish are taken only a few centimetres or tens of centimetres apart, this normalisation reduces the influence of the above-mentioned variables. Variability on the size scale of the petroglyph itself is taken into account by making multiple measurements (typically three to 12) within and adjacent to a given petroglyph, and variability on the microscale is averaged over by the spot size (8 mm) of the pXRF measurement.

The N_{Mn} and N_{Fe} results are shown as a scatter plot in Figure 4; the corresponding statistics are shown in Table 1; and the data from individual rock art elements are given in Table 2. We find that the N_{Mn} values on the rock art elements range from 0.5% ± 0.8% to 110% ± 9%, indicating that the varnish on some of the petroglyphs has reaccumulated to the same density

TABLE 2 D_{Mn}, D_{Fe} and N_{Mn} data for the rock art elements averaged over all spots measured on each element

Element ID	Motif	*N*	D_{Mn} (μg cm^{-2})		D_{Fe} (μg cm^{-2})		N_{Mn} (%)		
			Avg	SD	Avg	SD	Avg	SD	SE
CS1-1	Camel	5	226	16	256	25	92%	6.3%	3.2%
CS1-1e	Recently chiselled	1	1.4	0.7	278	28	0.6%	0.3%	–
CS2-1	Camel	3	124	59	194	46	68%	33%	23.0%
CS2-2	Wasm	3	17	1.9	284	14	12.1%	1.4%	1.0%
CS2-3	Arabic inscription, 1979 CE	6	3.8	0.8	333	11.6	3.5%	0.7%	0.3%
CS14-1	MSH inscription	3	55	6.1	331	27	33%	3.7%	2.6%
CS14-2	Small camel	3	58	17	328	22	30%	8.8%	6.2%
CSH-1	MSH inscription	4	57	18	292	23	34%	10.7%	6.2%
HC-1	Arabic inscription	4	54	4.6	101	23	28%	2.4%	1.4%
T7-2	Altarberg cross1	3	10.6	2.1	101	72	19%	3.9%	2.7%
T7-3	Altarberg cross 3	3	25	3.5	123	46	19%	2.7%	1.9%
T7-5	Altarberg cross 2	3	11.2	4.7	192	46	20%	8.5%	6.0%
T10-1-1	Ibex	4	230	88	230	25	108%	15%	8.9%
T10-1-2	Older ibex	3	258	38	292	57	97%	16%	11.0%
T10-2	Ibex with blood from nose	6	128	40	55	29	100%	28%	12.4%
T10-2f	Head of anthropomorph	3	159	22	46	16	99%	19%	13.7%
T14-1	Ibex	5	92	12.3	288	22	49%	6.5%	3.3%
T15-2-1	Ibex	4	209	36	135	51	86%	23%	13.0%
T15-2-2	Camel	4	194	40	116	9.6	95%	19%	11.2%
T19-1	Aurochs	7	314	41	278	34	106%	14.0%	5.7%
T19-2	Anthropomorph and spear	3	283	74	275	40	96%	25%	17.6%
T19-3	Circle	1	305	49	238	55	103%	25%	–
T20-1	Horn-tailed lizard	6	298	30	509	174	109%	11.1%	5.0%
T20-2	Small anthropomorph	1	60	19	284	27	19%	5.9%	–
T20-3	Hismaic letters	6	61	14	227	84	22%	6.1%	2.7%
T20-4	Ibex	2	243	5.4	345	25	89%	2.0%	2.0%
T20-5	Wasm	3	25	7.5	234	51	10.7%	3.3%	2.3%
T21-1	Feline	4	78	12.9	121	78	91%	18%	10.5%
T22	Human couple	6	188	48	142	36	84%	14.9%	6.7%
T23-1	Male anthropomorph (?)	4	71	17	115	24	49%	7.4%	4.3%
T23-2	Ibex	2	233	27	187	0.9	110%	8.6%	8.6%
T25-4	Ibex	3	31	9.8	259	134	10.1%	3.2%	2.3%
HFB-1	Arabic inscription, 2003 CE	1	1.2	1.9	115	108	0.5%	0.8%	–
HFB-2	Camel	4	145	24	145	64	105%	19%	11.1%
HFB-3	Anthopomorph	3	30	6.0	221	35	12.8%	2.6%	1.8%
KM-1	'Zissis 1940'	3	0.4	0.4	53	97	2.7%	2.9%	2.0%
KM-2	Cross and inscription	4	5.4	4.7	106	35	39%	34%	19.4%
KM-3	Cross, cell C, #1	3	4.1	1.0	72	29	3.4%	0.8%	0.6%
KHB1-1	Horse with rider	4	59	34	284	42	19%	10.7%	6.2%
KHB1-2	Ibex	3	83	3.2	269	50	33%	1.3%	0.9%
KHB1-3	Camel with rider	3	17	0.8	149	17	8.7%	0.4%	0.3%
KHB1-4	Camel	3	76	9.9	198	2.0	27%	11.7%	8.3%
KHB1-5	*Wusum*	3	22	2.4	150	19	9.0%	1.0%	0.7%

(Continues)

TABLE 2 (Continued)

Element ID	Motif	*N*	D_{Mn} (μg cm^{-2})		D_{Fe} (μg cm^{-2})		N_{Mn} (%)		
			Avg	SD	Avg	SD	Avg	SD	SE
KHB1-6	Ibex	3	47	4.7	168	18	15%	1.5%	1.1%
KHB1-7	Dog	3	123	9.1	317	77	38%	2.9%	2.0%
KHB2	Equestrian	3	6.9	0.9	152	78	2.9%	0.4%	0.3%
KHB3	Ibex	3	85	8.6	320	56	24%	2.4%	1.7%
JT1-1	Hismaic inscription	6	15	1.3	183	40	8.2%	2.0%	0.9%
JT1-2	Camel	3	25	2.2	156	52	17%	1.2%	0.8%
JT1-3	Hismaic inscription	3	68	6.5	418	53	33%	8.3%	5.9%

Note: Avg, arithmetic average; SD, standard deviation; SE, standard error.

as on the surrounding intact surface. This is in good agreement with the range observed for recent to Neolithic rock art in our study in the Ha'il region (Macholdt et al., 2018). In contrast, the N_{Mn} values in the Hima region, where the rock art dates mostly from the period following the onset of dry conditions *c*.5–6 ka BP, are < 40% (Macholdt et al., 2019). The N_{Fe} values range from 24% ± 23% to 333% ± 39%, which shows that Fe oxyhydroxides had accumulated on the petroglyph surfaces

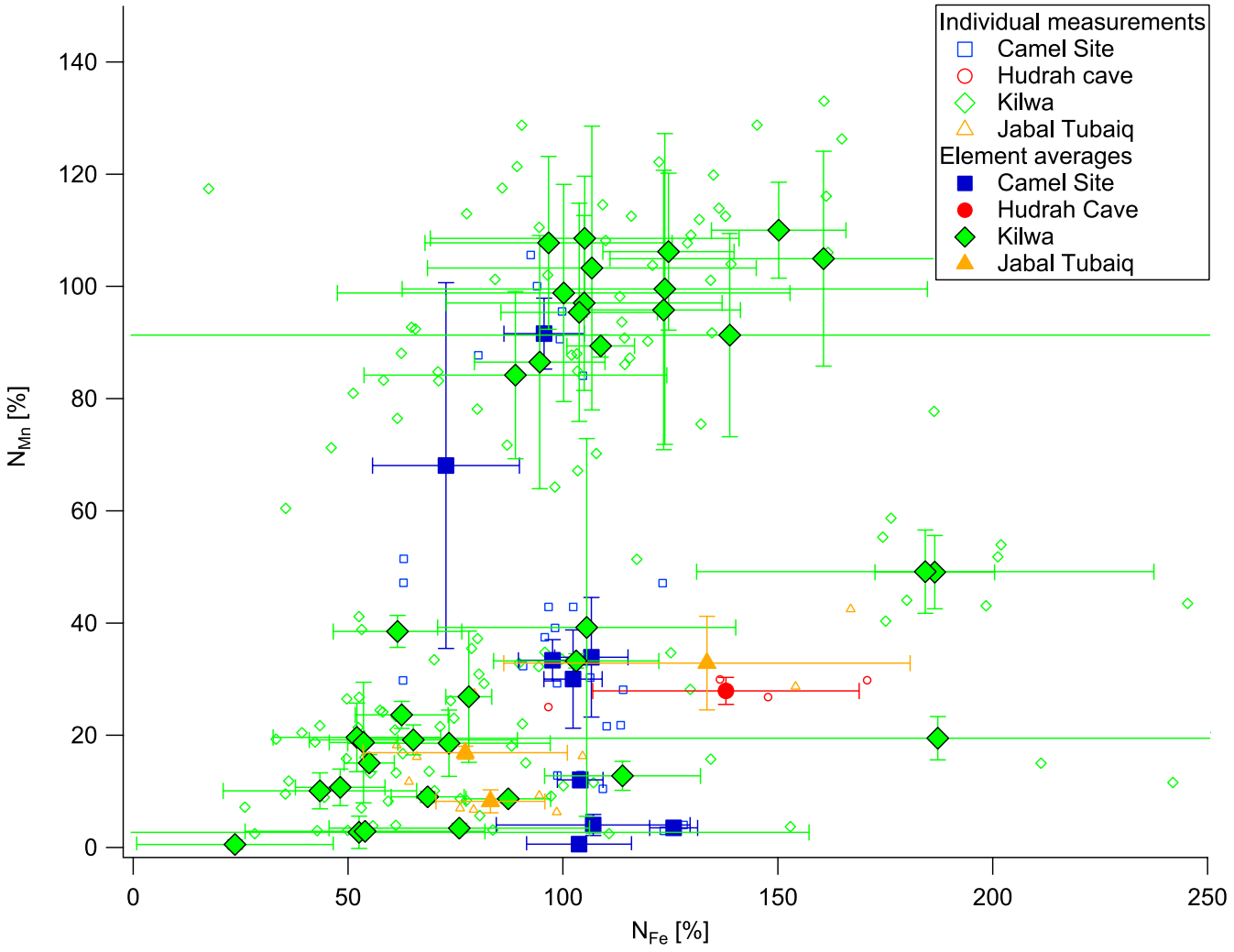

FIGURE 4 Normalised areal densities of Mn and Fe, N_{Mn} versus N_{Fe}, on the petroglyphs. The larger symbols with error bars indicate the averages and standard deviations of the measurements on each rock art element; smaller symbols are the individual spot measurements

to higher densities than present in the intact varnish. Even on the elements with very low amounts of Mn varnish regrowth, N_{Fe} is typically at or above about 50%, which suggests that Fe begins to accumulate before the deposition of Mn oxyhydroxides. This agrees with our previous observation of a positive Fe intercept in regression analyses of D_{Fe} versus D_{Mn}, which suggests the presence of an Fe oxyhydroxide layer at the base of the varnish. This layer might act as a catalyst for the formation of the Mn oxyhydroxides (Dorn, 2018; Macholdt et al., 2019). As in our previous work, we find no significant correlation between N_{Mn} and N_{Fe}, and no evidence of a relationship between N_{Fe} and the age of the rock art based on thematic considerations (Andreae et al., 2020; Macholdt et al., 2018, 2019). We will therefore focus our subsequent discussion on the varnish regrowth on N_{Mn}.

4.4 | Variability of the Mn and Fe areal densities

The great variability of varnish cover density, of both intact varnish and regrowing varnish on rock art, has been frequently pointed out in the literature and used as an argument against the possibility of using varnish density as a tool to estimate petroglyph age. This variability is clearly evident in Figures 3a,b, where individual measurements of D_{Mn} are shown to range from 12 to 415 μg cm^{-2} on intact varnish and from 0 to 400 μg cm^{-2} on the rock art. The widest range is found at Kilwa, as expected in view of the large sample size and diversity of varnished surfaces. For a quantitative analysis of this variability at different scales, we calculated the coefficients of variation (CV), that is, the ratio of the SD over the mean (expressed as a percentage), of the areal density measurements on the varnished surfaces. Table 1 shows that the variability of D_{Mn} of intact varnish at the site scale (tens of metres to a few kilometres) is in the range of 15–40%, similar to our previous observations (Andreae et al., 2020; Macholdt et al., 2019).

There is considerable variability of the varnish density at the microscale on the rock surfaces, ranging from the thickest varnish in microbasins through thin coatings on exposed quartz grains to the total absence of varnish on recently eroded or spallated surfaces (Cremaschi, 1996; Liu & Broecker, 2007; Zerboni, 2008). Since the pXRF measurements cover a spot of 8 mm diameter, much of this variability is averaged over in this type of analysis. The variability at the scale of the rock art elements (centimetres to metres) can be derived from the statistics of replicate measurements on the individual elements. Typically, on each element, several measurement spots were selected (identified by arrows in Fig. S1 in the additional supporting information) and at each measurement spot, two to five measurements were made close to one another (within a few millimetres). Measurements on intact varnish were made the same way, typically in the form of two to five replicates close to the corresponding spots in the rock art element. When the measurements on the intact varnish spots were not significantly different, the intact varnish data were pooled for a given element. Thus, on average, there are seven measurements representing the adjacent intact varnish for each spot or element, and the average CV of these measurements is 15% (n = 97; range = 1–61%). The uncertainty of the mean for each group of measurements is represented by the relative SE, which on average was 9.8% (range = 1–46%). On the rock art elements themselves, we made on average 2.6 replicate measurements on each spot, with an average CV of 12% (N = 184, range = 0.2–72%) and average SE of 9.8% (range = 0.2–51%) (four values with CV > 100% were not included because they were from measurements very close to zero and thus have a large relative error in spite of a small absolute error).

The uncertainty of the normalised densities, N_{Mn}, is derived using SE propagation from the SEs of the measurements on the petroglyph spots and the corresponding intact varnish measurements. The average relative SE of the N_{Mn} values is 18% (N = 173, range = 2.5–53%). The SEs for the measurements on the individual rock art elements are given with the corresponding D_{Mn} and N_{Mn} values in Table 2.

4.5 | Absolute and normalised Mn and Fe accumulation rates

We derived the effective or apparent element accumulation rates, R_{Mn} and R_{Fe}, by dividing the areal density of Mn or Fe by the known or estimated exposure age of the rock art surface (Table 3). This rate is the average elemental accumulation on the rock surface over the time it has been exposed, and as such averages over potential variations of the true, instantaneous accumulation rate with time. We use the term 'apparent' to reflect this potential time dependence and the possibility that, in the long run, deposition is likely to compete with the removal of varnish by erosion and weathering of either the varnish itself or of the underlying rock.

The youngest surfaces include a chisel mark from CS made within the last decade, Arabic inscriptions with dates corresponding to 1979 and 2003 CE, and an inscription from 'Zissis 1940' at Kilwa monastery. The D_{Mn} values on these inscriptions are very low, and thus the accumulation rates derived from them have a very high uncertainty, with R_{Mn} values ranging from 5 ± 5 to 140 ± 160 μg cm^{-2} ka^{-1}. The Zissis inscription is particularly questionable since it is on the outside of one of the monastery cells at Kilwa, and may have been altered by later visitors. The other rates on young surfaces are relatively high, consistent with our previous observations that a small amount of Mn varnish forms relatively rapidly (within decades) on freshly cleared

TABLE 3 Mn and Fe areal density (D_{Mn} and D_{Fe}), apparent Mn and Fe accumulation rates (R_{Mn} and R_{Fe}), and normalised accumulation rates (R_{NMn}) on inscription surfaces with known or estimated ages

Element ID	Element	Age (ka)	D_{Mn} (μg cm^{-2})	D_{Fe} (μg cm^{-2})	R_{Mn} (μg cm^{-2} ka^{-1})	R_{Fe} (μg cm^{-2} ka^{-1})	N_{Mn} (%)	R_{NMn} (% ka^{-1})
CS1-1e	Recently chiselled	0.01 ± 0.01	1.4 ± 0.7	280 ± 28	140 ± 160	28,000 ± 28,000	0.6% ± 0.3%	58 ± 65
HFB-1	Arabic, 2003 CE	0.015 ± 0.001	1.2 ± 1.9	115 ± 108	76 ± 120	7200 ± 6800	0.5% ± 0.8%	33 ± 52
CS2-3	Arabic, 1979CE	0.039 ± 0.001	3.8 ± 0.8	330 ± 12	95 ± 20	8300 ± 400	3.5% ± 0.7%	87 ± 19
KM-1	'Zissis 1940'	0.078 ± 0.001	0.4 ± 0.4	53 ± 97	4.7 ± 5.0	670 ± 1200	2.7% ± 2.9%	34 ± 36
HC-1	Arabic, 6th–8th centuries CE	1.3 ± 0.2	54 ± 5	101 ± 23	41 ± 7	78 ± 21	28% ± 2%	22 ± 4
CS14-1	MSH inscription	2.0 ± 0.3	55 ± 6	330 ± 27	28 ± 4	160 ± 20	33% ± 4%	17 ± 3
CSH-1	MSH inscription	2.0 ± 0.3	57 ± 18	290 ± 23	28 ± 9	150 ± 20	34% ± 11%	17 ± 6
T20-3	Hismaic inscription	2.0 ± 0.3	61 ± 14	230 ± 80	31 ± 8	110 ± 40	22% ± 6%	11 ± 3
JT1-1	Hismaic inscription	2.0 ± 0.3	15 ± 1.3	180 ± 40	7.7 ± 1.0	91 ± 22	8.2% ± 2.0%	4.1 ± 1.1
JT1-3	Hismaic inscription	2.0 ± 0.3	68 ± 6	420 ± 53	34 ± 5	210 ± 30	33% ± 8%	16 ± 4
	Average, Arabic and Hismaic inscriptions		52 ± 18	260 ± 110	28.3 ± 11.2	134 ± 49	26.3% ± 10.0%	14.4 ± 6.1
	Ha'il region, south Arabia[†]	–	–	–	17 ± 14	60–100	–	12 ± 3
	Hima region, south Arabia[‡]	–	–	–	13 ± 10	110–200	–	10 ± 3
	Owens/Rose Valley, California[§]	–	–	–	15–21	6–11	–	~10

Notes: Values are averages and standard deviations.

[†]From Macholdt et al. (2018).

[‡]From Macholdt et al. (2019).

[§]From Andreae et al. (2020).

surfaces (Andreae et al., 2020; Macholdt et al., 2017a, 2018, 2019).

The older inscriptions include an Arabic inscription from the Early Islamic period, which based on its script style (old Kufic) has been dated to the seventh to ninth centuries CE (Frédéric Imbert and Ilkka Lindstedt, personal communications, 2020). Two inscriptions from CS are in the MSH script (Jérôme Norris, personal communication, 2020). One inscription from Kilwa and two from JT are in the Hismaic script (Jérôme Norris and Michael Macdonald, personal communications, 2020). Inscription T20-3 at HFB had been transcribed and analysed by Harding and Littmann (1952).

The dating of the Hismaic and MSH scripts is relatively uncertain, but both were used predominantly between *c*.100 BCE and 100 CE, with their use declining to *c*.300 CE (Macdonald, 2004; Norris, 2018). For the purpose of calculating an accumulation rate on these inscriptions, we assign an age of 2.0 ± 0.3 ka to both Hismaic and MSH scripts. With one exception (JT1-1), the Hismaic and MSH inscriptions yield very similar accumulation rates in the range of 28–34 μg cm^{-2} ka^{-1}, in spite of coming from three relatively widely dispersed sites. The Arabic inscription HC-1 suggests a slightly higher rate, 41 ± 7 μg cm^{-2} ka^{-1}, but given that we only have one sample of this age, it is not clear whether this difference is significant. The average rate from the Arabic, MSH and Hismaic inscriptions is 28 ± 11 μg cm^{-2} ka^{-1} (95% confidence interval = 18–38 μg cm^{-2} ka^{-1}), which is the value that we will use below as a basis for estimates of petroglyph ages. This rate is somewhat higher than, but still comparable with, the rates we measured previously at sites in Arabia and California (13–21 μg cm^{-2} ka^{-1}) (Table 3).

The Fe accumulation rates show a similar pattern, with very high rates for the youngest surfaces suggesting fast initial accumulation and lower rates on the older inscriptions. The extremely high value on CS1-1e may be the result of some Fe oxides remaining from an incompletely removed sub-surface Fe enrichment. The mean R_{Fe} of 134 ± 49 μg cm^{-2} ka^{-1} on the older inscriptions is also in the range of previous observations.

The normalised Mn accumulation rate, R_{NMn}, is calculated analogously to the absolute accumulation rate by dividing N_{Mn} by the age of the surface. This value can be interpreted as a 'revarnishing rate', that is, the rate (in per cent per 1000 years) at which the varnish on a petroglyph surface approaches that of the surrounding intact varnish.

In our previous studies, we had found that this rate showed less variability around the mean than the corresponding absolute accumulation rates, because the normalisation takes into account much of the variability caused by the numerous microenvironmental factors influencing varnish growth. The average R_{NMn} from the Arabic, MSH and Hismaic inscriptions is 14.4 ± 6.1% ka^{-1} (95% confidence interval = 9.4–19.3% ka^{-1}), which is the value that we will use below as basis for estimates of petroglyph ages based on the normalised data. This rate is slightly higher, but not significantly different from, those measured previously at our sites in Arabia and California (10–12% ka^{-1}) (Table 3), a quite striking result considering the large differences in geographical locations between these sites.

This fact implies that, assuming a linear model, after *c*.7–8 ka, the varnish on the rock art becomes indistinguishable from its surroundings. At this point, the rate of varnish loss by weathering equals the rate of varnish accumulation. In our previous papers, we found that this 'taphonomic limit' is reached at ages around *c*.10 ka (Andreae et al., 2020; Macholdt et al., 2018, 2019). In reality, it may take somewhat longer to reach full revarnishing, because our evidence, especially from California, indicates that the rate of revarnishing slows over time, so that a non-linear growth model may be more realistic. Unfortunately, however, so far we have not been able to quantify this non-linear behaviour because of the lack of dated surfaces spanning the entire range of ages. Our previous work has shown, however, that an assumption of linear growth results in reasonable age estimates on millennial scales up to *c*.10 ka.

4.6 | Rock varnish on petroglyph surfaces

For our study, we made measurements on 51 rock art elements, representing a broad sample of the rock art motifs that occur in the study region. (An 'element' is a single form or design unit, often used synonymously with 'petroglyph'. A 'motif' is an element often used within a given corpus and is related to a particular style, for example, an ibex or a camel.) Examples of the rock art are shown in Figure 5; images of the complete set of measured elements are provided in Supplement S1 in the additional supporting information. The D_{Mn}, D_{Fe} and N_{Mn} values are listed in Table 2; the N_{Mn} data are plotted in Figure 6 grouped by motifs. In Figure 6, the different study sites are distinguished by symbol shape and colour. The scale on the right side of Figure 6 represents age estimates for the elements using the revarnishing rate, R_{NMn}, of 14.4% ka^{-1} derived above.

Considering the entire data set, the N_{Mn} values and corresponding age estimates cluster into two ranges (Fig. 6). The first cluster is in the range between about 80% and 110% (6–9 ka BP), corresponding approximately to the later part of the PPNB and the LN, with subsistence based on hunting and the development pastoral nomadism. The second cluster is below about 50% N_{Mn}, beginning around the Late Bronze Age (*c*.4 ka BP), when the subsistence had shifted to pastoral nomadism, oasis agriculture and later camel-based trade, and extending to the present. Similar to observations from all across Arabia, there appears to be a prominent gap between these two periods, when rock art creation underwent a long and pronounced reduction in volume (Khan, 2007). The elements corresponding to the PPNB/LN period are concentrated at HFB at Kilwa and the camel reliefs at CS. The concentration of Neolithic elements at HFB is consistent with the abundance of lithic material of PPNB age observed at this site by Rhotert et al. (1938) (subsequently referred to as R38). In the following, we will discuss the elements grouped in motif clusters. It should be noted, however, that the true ages of the PPBN/LN cluster elements could be somewhat higher than suggested by their N_{Mn} values, because our assumption of a linear Mn accretion rate ignores the potential slow-down of varnish accretion with age.

4.6.1 | Neolithic game animals

Group Neolithic game animals comprises three elements: a very large bovid (T19-1; Fig. 5b), a horn-tailed lizard (T20-1; Fig. 5a) and a feline (T21-1). (Our sample code refers to the figures in R38, such that T19 refers to *Tafel* (= plate) 19 in R38, etc.). The bovid image T19-1 (Fig. 5b) is probably the most famous figure at Kilwa, which has been interpreted as an aurochs (*Bos primigenius*), the wild ancestor of domesticated cattle (Guagnin et al., 2016; Horsfield et al., 1933). Below this image is a human holding what may be a spear that penetrates the side of the bovid (T19-2). Attached to the hind leg of the bovid is a line leading to a circle (motif group abstract, T19-3), which has been interpreted as a tie-down by R38. The varnish densities on these three images (106% ± 14%, 103% ± 25% and 96% ± 25% for bovid, circle and human, respectively—connected by a thin line in Fig. 6) are not significantly different, and thus it is possible they may have been created together. Bovid hunting during the PPN has been documented through archaeological evidence and rock art from several sites in Arabia and the Levant; for example, rock art from southern Iraq suggests the presence of both domestic and wild bovids in hunting scenes (Zarins, 1990).

Element T20-1 has been interpreted by R38 as a horn-tailed lizard. It is located on a prominent rock on top of HFB, on which there are also small human figures and numerous Hismaic inscriptions (see below), some of which are superimposed on the lizard. Its N_{Mn} is very close to that of the aurochs, suggesting that it also dates from the PPNB/LN.

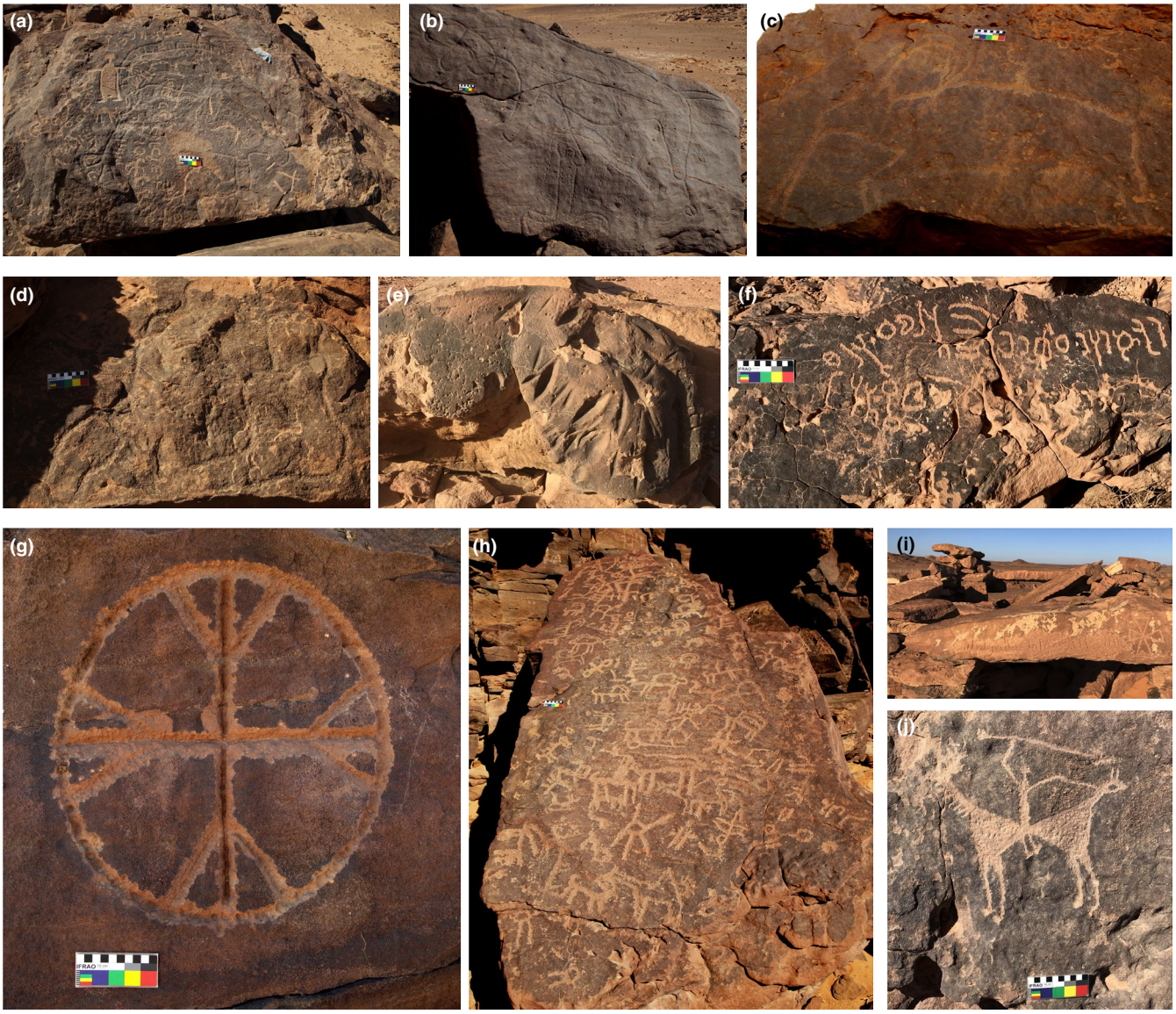

FIGURE 5 Examples of the rock art elements investigated (see the text for a discussion): (a) composite panel with an horn-tailed lizard (HFB, T20); (b) bovid (T19-1, HFB); (c) ibex (T10-2, HFB); (d) embracing human couple (T22, HFB); (e) camel in relief (CS1-1, Camel Site); (f) Hismaic inscription (JT1-1, Jabal Tubaiq); (g) cross symbol (T7-2, Altarberg); (h) composite panel (KHB1, KHB); (i) Kufic inscription and cross (KM-2, Monastery); and (j) equestrian with lance (KHB-2; KHB)

Element T21-1 appears to be a feline, represented in a very simple style (alternatively, it has been interpreted as an ox by Horsfield et al., 1933). Its N_{Mn} (91% ± 18%) suggests a similar age to other representations of Neolithic wild fauna, but the very uneven intact background varnish results in a relatively large uncertainty.

4.6.2 | Ibex

Group ibex contains the largest number of elements, consistent with the high frequency at which this motif is represented in Arabian rock art (Guagnin et al., 2016, 2017; Khan, 2007). At HFB, six of seven ibex elements have an N_{Mn} consistent with PPNB/LN ages, whereas at KHB, the ibex elements all plot in the period after the onset of drought. This suggests that the ibex (*Capra ibex*), as a prestige game animal, was hunted and depicted in rock art throughout the human presence in Arabia, similar to the findings we had made previously in the Ha'il region (Macholdt et al., 2018), particularly at Shuwaymis (Guagnin et al., 2015). Interestingly, this has an analogue in south-western North America, where the bighorn sheep (*Ovis canadensis*) is also the species most commonly represented in rock art throughout human history (Andreae et al., 2020; Garfinkel et al., 2010; Rogers, 2010; Whitley & Dorn, 2007).

An ibex image on the eastern side of HFB (T10-2; Fig. 5c) shows two lines emanating from its mouth which have been

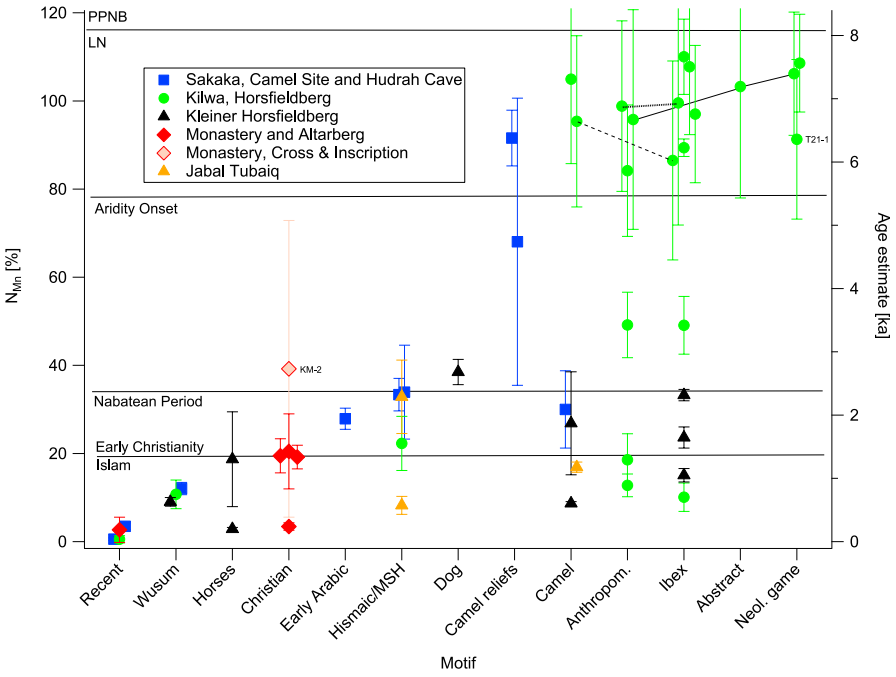

FIGURE 6 Normalised areal densities, N_{Mn}, and age estimates (right *y*-axis) of the rock art elements grouped by motifs

interpreted as blood streams (R38), indicating a kill of this animal in conjunction with a hunt or sacrifice. On its back is a small human figure (T10-2f), which has the same N_{Mn} value as the ibex (99% ± 19% versus 100% ± 28%, respectively; symbols connected by a dotted line in Fig. 6). A near-horizontal slab on the top of HFB contains two ibex images, one superimposed on the other. The older element (T10-1-2) has a somewhat lower N_{Mn} (97% ± 16%) than the superimposed and thus younger ibex element (T10-1-1; 108% ± 15%); however, this difference is not statistically significant and serves to highlight the limited temporal resolution achievable with our technique.

The highest N_{Mn} is associated with a fragmentary ibex image, where only the horns can be distinguished (T23-2; 110% ± 9%). It is on the same surface as the possible anthropomorph T23-1, but the large difference in varnish density argues against any connection between the two images. Two ibex images show slightly lower N_{Mn} (T15-2-1: 86% ± 23%; T20-4: 89% ± 2%), but are still well within the range of values consistent with a PPN/LN age. The ibex T15-2-1 is on the same surface as a camel with comparable N_{Mn} (T15-2-2: 95% ± 19%; connected by a dashed line in Fig. 6), while T20-4 is on the same panel as the horn-tailed lizard. The lizard is superimposed on the ibex, but here again, the lower, older element has an apparently lower N_{Mn} than the superimposed, younger element.

An intermediate N_{Mn} on an ibex from HFB was measured on an isolated image on a vertical wall on the western side (T14-1: 49% ± 6%). This figure has an oval behind it with an N_{Mn} indistinguishable from that of the animal, which is probably part of the same representation and for which there is no conclusive interpretation (R38). A small ibex figure with short horns (T25-4) is located near the top of HFB. It has very light varnishing and is very different in size and style from the other ibex images on HFB and must belong to a more recent phase of rock art creation. Nearby is an anthropomorph (HFB-3) with a very similar degree of revarnishing.

Also clearly distinct, in both the degree of revarnishing and the style of representation, from the older ibex images of HFB are the three ibex elements on the hill at KBH. The ibex on KHB are much smaller, tend to have exaggerated horns and are much less naturalistic than those from HFB, especially KHB3, where the body is reduced to a horizontal line. KHB1-2 and KHB1-6 are on the same slab as the majority of images measured at KHB, and show N_{Mn} comparable with these images, suggesting they are roughly contemporaneous and possibly associated with the period of camel trade.

4.6.3 | Anthropomorphs

We have already mentioned two PPNB/LN anthropomorphs from HFB, the human associated with the aurochs (T19-2: 96% ± 25%) and the figure T10-2f (99% ± 19%), the small human on top of the ibex T10-2. A third human representation, which is probably also of PPNB/LN age, is that of a seated embracing couple (T22: 84% ± 15%; Fig. 5d). This unique image is produced in a slightly three-dimensional form, using the shape of the rock substrate. It was assigned a PPN age by R38, who observed a close resemblance of this image to a limestone statuette found in a cave in Wadi Khareïtoun near Jerusalem. The woman in this image appears to be six-toed, which Zarins (1990) relates to a PPNB statuary fragment from 'Ain Ghazzal, Jordan. Overall, however, human figures are quite rare at

Kilwa in comparison with our other sites from north-western Arabia, for example, Jubbah, where a large number of hunting and dancing humans are represented.

Element T23-1 is difficult to interpret: It could be a stylised male human figure (R38) or an abstract representation. Its degree of varnishing suggests an intermediate age between the LN and Iron Age periods.

A small human figure with horizontally outstretched arms and widely spread fingers (T20-2: 19% ± 6%) is found on the same panel as the horn-tailed lizard. It is wearing a long tunic, reaching down to its feet and what appears to be some sort of belt and sash. Its N_{Mn} is identical to the Hismaic writing which surrounds it on the same panel, and it may thus have been created around the turn of the Common Era. Nearby, also near the top of HFB, is a small human figure with legs seen side on and arms out to the side, with his hands on the hips. It is only lightly varnished (13% ± 3%), and in close proximity to the small ibex HFB3, with a similar N_{Mn}.

4.6.4 | Camels

The dromedary camel (*Camelus dromedarius*) has played a central role in Arabia throughout human history, first as a hunting prey and, following its domestication *c*.3000 BP, as the basis of a herding economy and means of trade and transportation. It is thus not surprising that it is represented in rock art throughout the ages (Khan, 2007). At HFB, we made measurements on two camel elements, both with very high N_{Mn}. One, T15-2-2, is on the same panel as ibex T15-2-1, and has a similar N_{Mn} (95% ± 19% and 86% ± 23%, respectively), and the other camel element (HFB-2) also has a very high N_{Mn} of 105% ± 19%. These two images already impressed R38, who commented on their realistic, almost three-dimensional representation, which is completely different from the very abundant later camel representations, which tend to be very stylised, often with triangular or semi-circular bodies, and assigned them a Neolithic age.

Even more remarkable in their style of execution are the haut-relief camel images from the Sakaka CS, with their very detailed and naturalistic representation (Charloux et al., 2018). One of these animals, CS1-1, has N_{Mn} nearly identical (92% ± 6%; Fig. 5e) to the Neolithic camels at Kilwa. The other, CS2-1, has yielded both very high (106% ± 8%) and relatively low (30–52%) values. This high variability is most likely due to the extremely exposed position of this image on the top of a cliff, with a very high chance of wind erosion and weathering. Given that weathering processes can only remove varnish, but that there is no known process to add varnish to an exposed rock face artefactually, we feel that the high value is more likely to be representative of the age of this image, and that a PPNB/LN age is most plausible for both images.

The PPNB/LN camel images at Kilwa and CS are separated by a huge gap in both representational style and degree of varnishing from the post-domestication images at these two sites and JT. Two camels at KHB are on the same highly decorated slab and show the typical stylised representation, with four stick legs and triangular or semi-circular bodies. The camel with the triangular body (KHB1-4: 27% ± 12%) has close parallels to similar images at Shuwaymis with estimated ages *c*.3000 BP, while the very stylised camels with semi-circular bodies (CS14-2: 30% ± 9% and JT1-2: 17% ± 1%) resemble younger images at Jubbah and Shuwaymis (Macholdt et al., 2018). The most lightly varnished image (KHB1-3: 8.7% ± 0.4%) appears to have a rider on its back. The similarity in the style of representation and age estimates between Kilwa and the Ha'il region may reflect cultural exchange along trade routes during the time of the camel caravan trade.

4.6.5 | Dogs

Dogs have been part of hunting strategies in Arabia since at least 9000 BP, even predating the Neolithic transition (Guagnin et al., 2018a). A single image of a dog (KHB1-7) was found on the large panel at KHB (Fig. 5h). It is relatively heavily varnished (38% ± 3%), but within the range of uncertainty of the other images on this rock slab. It is stylistically very different from the Neolithic dog representations in the hunting scenes at Shuwaymis (Guagnin et al., 2018a; Macholdt et al., 2018), but overlaps in N_{Mn} value some of the dog images from that site.

4.6.6 | Inscriptions

Above, we have already discussed the Hismaic, MSH and early Arabic inscriptions that provide the basis for our varnish growth rate and age estimates (Fig. 5f). Figure 6 shows that, with the exception of one case at JT, the MSH and Hismaic inscriptions cluster quite closely together in spite of the substantial geographical distances, consistent with their use by nomads. They span a range of age estimates in accordance with the estimated length of time that they were in use (the average is, of course, by definition the same as that of the middle of that period). The early Arabic inscription from HC yields a somewhat older age estimate than expected, but given the exposed character of this site and the uncertainty of the varnish growth rate, this is not likely to be significant.

The famous inscription in early Arabic (Kufic) script on a lintel in Kilwa monastery (KM-2; Fig. 5i), already mentioned by Bell from her 1914 visit, yields an estimated age that is obviously too high (*c*.3000 BP or 1000 BCE; the light red symbol on Fig. 6). This inscription and the cross that appears next to it have been identified as being part of an Early Christian monastic culture, which flourished at Kilwa on the eve of Islam, with a tentative age of *c*.1000–1300 BP (Farès,

2011; Hoyland, 2017). Examination of the photograph of this inscription explains this artefact. Traces of plaster above and beside the inscription indicate that it may have been covered in plaster for part of the time after its creation. Also, by comparison with the area around the cross, the area surrounding the inscription looks like it has been cleared of varnish, thus rendering invalid the assumption of an intact reference varnish. Finally, the architectonic evidence suggests that this inscription has been inside a building until the collapse of the building's structure. All these factors unfortunately render it impossible to derive a valid age estimate from our measurements for this interesting inscription.

As mentioned above, the inscriptions in Arabic and Latin script (HFB-1, CS2-3 and KM-1) dated from within the last 80 years, all yield N_{Mn} age estimates near zero. While this points out one of the limitations of our method, that is, the inability to obtain age estimates for very young surfaces, it also provides evidence for our underlying assumption that surfaces with near-zero age also have near-zero N_{Mn} and D_{Mn} values.

4.6.7 | Christian symbols

We conducted measurements on four cross symbols that are plausibly related to the Christian monastic activity documented at Kilwa (Bell, 1927; Farès, 2011; Horsfield, 1943; Horsfield et al., 1933; Rhotert et al., 1938). Christianity arrived in the region in the early part of the first millennium CE, with several Bedouin tribes converting to Christianity (Gilmore et al., 1982), while Islam was established at Dumat al-Jandal, beginning in 626 CE by raids led by Prophet Muhammad and consolidated *c*.634 CE under first caliph Abu Bakr (Charloux & Loreto, 2013). It may have taken even longer for Islam to spread to remote locations such as Kilwa, and Christianity appears to have coexisted with Islam in northern Arabia for some time (Hoyland, 2017). The three crosses on the side of the AB facing the monastery (T7-2, T7-3 and 7-5; Fig. 5g) all have N_{Mn} values very close together and yield age estimates *c*.1.4 ka BP, in close agreement with the period expected for Christian activity in the region, and in particular with the date of 1.3 ka BP estimated on the basis of epigraphic evidence for the inscription and cross in the monastery (Hoyland, 2017). In contrast, a cross on a loose slab inside cell C #1 (KM-3), which was unearthed by the French–Saudi team (Farès, 2011), has a very low N_{Mn}, consistent with its lack of exposure by being underground or inside a cell for much of the time.

4.6.8 | Horses

The horse was domesticated *c*.4000–3000 BP and its use became widespread in Arabia *c*.2400 BP (Khan, 2007; Olsen, 2013). Our data set contains two horse images, both from KHB. One is an extremely stylised, small image of a horse with rider (KHB1-1) from the large slab KHB1 (Fig. 5h), which has an N_{Mn} suggesting an age within the same range as the other images on the slab (1–2 ka BP). The other, on the east side of KHB (KHB-2; Fig. 5j), shows a horse with an hourglass-shaped body and a rider who holds a weapon, probably a lance with a spearhead on the right, over his head. It resembles equestrian images documented by R38 from one of the outlying sites at Kilwa ('Stelle B') and from El Quweira (Al-Quwayrah, Jordan), shown on plate 27 in R38. Similarly shaped horses, often as part of battle scenes, have been observed at other sites, for example, at Hima and Sakaka, and have been attributed to the Islamic period (Gilmore et al., 1982; Macholdt et al., 2019; Olsen, 2013; Robin, 2018).

4.6.9 | Wusum

Wusum (singular *wasm*) are markings typically consisting of three characters, indicating tribal affiliation or property, and each tribe in Arabia has its own *wasm*. *Wusum* have been in continuous use for the marking of cattle, camels and tribal boundaries for thousands of years (Bednarik & Khan, 2005; Khan, 2013; McCorriston & Martin, 2010), and may have derived from cattle markings that can be seen on petroglyphs made as early as 7000 to 5500 BP (Khan, 2007). In our data set, there are three *wusum*, one each from CS (CS2-2), HFB (T20-5, in the panel with the horn-tailed lizard) and KHB (KHB-1-5, on the large panel KHB1). Their N_{Mn} cluster closely together, around 9–12%, suggesting ages of *c*.600–800 a. This falls within the age range of *wusum* we measured in the Hima and Ha'il areas (200–3000 a), consistent with the long use of this type of marking in Arabia (Khan, 2007).

Figure 7 shows the D_{Mn} data from the petroglyphs grouped in the same way as the N_{Mn} values in Figure 6. The advantages of the normalisation procedure are immediately evident. While the D_{Mn} values of the PPN/LN elements from HFB also mostly fall into the range before the onset of aridity, they scatter over a much wider range and some of them, particularly those on horizontal surfaces, reach implausibly old age estimates. The feline T21-1, on a vertical panel where the varnish on both the intact background and the petroglyph are fairly light, shifts to an unrealistically young age. The same applies to the cross symbols on the vertical panels on AB, where background and petroglyphs are lightly varnished. The high D_{Mn} value on horizontal surfaces and low values on highly inclined surfaces reflect the dependence of the rate of varnish accretion on surface inclination, which we have documented at sites in the Mojave Desert (Andreae et al., 2020). On the other hand, the cross

and inscription KM-2 in Kilwa monastery, where both the petroglyph and background had been subject to varnish removal, does not show an artificially high 'age', as it does in the N_{Mn} plot.

In summary, in our study area the measurements of varnish density on the rock art suggest two major phases of artistic and presumably socioeconomic activity, the first associated with hunting and herding activities in the PPN/LN, and the second reaching from the Bronze/Iron Age transition to the present, consisting of a mixture of hunting, camel herding and trading, monastic activity, and finally exploration and tourism. They are separated by a long period with little activity, beginning at the onset of aridity and extending through most of the Bronze Age. The elsewhere very common representations of humans with Bronze Age weapons, especially the characteristic lunate pommel-handled daggers (Anati, 1968; Macholdt et al., 2019; Magee, 2014a; Newton & Zarins, 2000), are conspicuously absent at our sites. Also notable is the scarcity of human representations in comparison with the large numbers of Neolithic dancers and hunters at Jubbah and at sites in south-eastern Jordan (Betts, 1987). Rhotert (R98) already commented of the low diversity of Neolithic animal species representations at Kilwa, which is in stark contrast to the diverse assemblages at other northern Arabian sites (Guagnin et al., 2016, 2017, 2018b). Especially surprising is the complete lack of gazelle images, considering that gazelle hunting was a very important component of the hunting economy in the PPN up to *c*.8000 BP and is frequently represented in rock art north of the Saudi Arabian border (Betts, 1987; Zarins, 1990).

5 | SUMMARY AND CONCLUSIONS

We measured by portable X-ray fluorescence (pXRF) the areal density of Mn and Fe in the rock varnish deposited on petroglyphs, inscriptions and on adjacent intact varnish at the Camel Site (CS) and Hudrah Cave (HC) (Sakaka, al-Jawf province), at Kilwa, and at a site in the Jabal Tubaiq hills (Tabuk province) in north-western Saudi Arabia. These measurements were complemented by femtosecond laser ablation inductively coupled plasma mass spectrometry (fs-LA-ICP-MS) analyses of varnish samples collected near the rock art sites.

The chemical composition of the varnish was characteristic of type I varnish, according to the classification proposed by Macholdt et al. (2017b). Mn, Fe, Al and Si were found to be the dominant elements, reflecting a mixture of Mn/Fe oxyhydroxides, clay minerals and quartz grains. The average Mn/Fe mass ratios at the different sites ranged between 0.60 ± 0.38 and 0.85 ± 0.62, typical of varnish grown under predominantly arid conditions. The trace element analysis showed the characteristic enrichment pattern, with strong enrichments of Mn, Pb, Ba, Co and Ce relative to the average crustal composition. Noteworthy was an unusually high Cu enrichment, which may be related to ancient copper mining and smelting in the region upwind of the study sites.

The Mn areal densities on the intact varnish, measured by pXRF, were similar at the four sites with an overall average of 209 ± 78 μg cm^{-2}. This value is significantly higher than our previous results in Saudi Arabia, with 105 ± 55 μg cm^{-2} in the Hima region (Macholdt et al., 2018) and 156 ± 94 μg

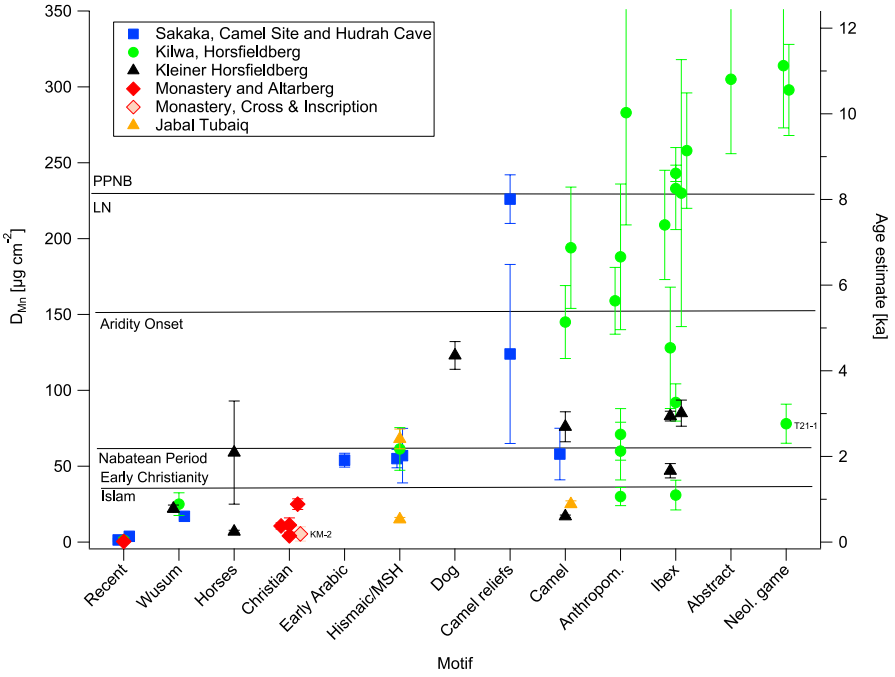

FIGURE 7 Areal densities, D_{Mn}, and age estimates (right *y*-axis) of the rock art elements grouped by motifs

cm^{-2} in the Ha'il region (Macholdt et al., 2019). The reasons for this difference are unclear, but may be related to differences in the weathering resistance of the rock substrate. The Mn densities on the rock art span from zero on freshly cleared surfaces to values identical to the surrounding intact varnish for the oldest rock art elements.

We define the normalised Mn areal density, N_{Mn}, as the ratio (%) between the Mn density on a rock art element to that of the surrounding intact varnish. This variable can be understood as the degree to which varnish has regrown on the rock art element over time to match the surrounding original varnish. At our sites, N_{Mn} ranged from zero to values around 100%, with a clear correlation to the known or inferred age of the rock art. The lowest values were found on recent graffiti with ages of a few decades, the highest on rock art thought to be of Pre-Pottery Neolithic B (PPNB)/Late Neolithic (LN) age based on archaeological considerations.

We used D_{Mn} and N_{Mn} measured on Hismaic, Mixed Safaitic–Hismaic (MSH), and early Arabic inscriptions to derive estimates of the Mn accumulation rates by dividing the Mn areal densities by the estimated ages of the rock art elements. The average absolute accumulation rate, R_{Mn}, based on these inscriptions is 28 ± 11 μg cm^{-2} ka^{-1} (95% confidence interval = 18–38 μg cm^{-2} ka^{-1})—somewhat higher, but still comparable with, the rates we had measured previously at sites in Arabia and California (13–21 μg cm^{-2} ka^{-1}). The normalised Mn accumulation rate, R_{NMn}, calculated by dividing N_{Mn} by the age of the inscriptions, averaged $14.4 \pm 6.1\%$ ka^{-1} (95% confidence interval = 9.4–19.3% ka^{-1}), also slightly higher, but not significantly different from those measured previously at our sites in Arabia and California (10–12% ka^{-1}). This similarity is quite striking, considering the large differences in geographical locations between these sites. Using these absolute and normalised accumulation rates, we could derive age estimates for rock art elements of unknown age. We caution, however, that these age estimates are quite uncertain in absolute terms (95% confidence interval = about ±40%) because of the limited number of calibration surfaces and the assumption of a linear growth rate, as well as the potential interference of site-specific variables other than time that may have affected varnish growth. For the oldest elements, our age estimates may be too low, given the evidence from previous studies that varnish accumulation slows down with age (Andreae et al., 2020).

Our measurements on the petroglyphs clustered into two ranges of Mn densities and corresponding ages, one covering the PPNB and LN (*c*.8 to 6 ka BP), the other reaching from the Bronze/Iron Age transition (*c*.4 ka BP) to the present, with few values in between. The PPNB/LN material was concentrated at the Horsfieldberg (HFB) site at Kilwa and the camel reliefs at CS, whereas the Bronze to Iron Age art was present across all sites. The PPNB/LN ages estimated for the rock art at HFB are in good agreement with the estimates of Rhotert et al. (1938), who had proposed an Upper Neolithic age based on his archaeological findings. The PPNB/LN rock art motifs at HFB include a range of game animals, including aurochs, ibex and camel. There are several anthropomorphs, some of which could be interpreted as hunters with spears, as well as an embracing human couple. Further motifs comprise a horn-tailed lizard, and some elements with inconclusive meaning. The camel reliefs at CS are unique in North Arabian rock art, as their N_{Mn} values clearly indicate a Neolithic age, in contrast to the otherwise two-dimensional representations from that period.

The early inscription material from our sites dates from the turn of the Common Era, using Hismaic and MSH scripts. Later inscriptions come from the Early Christian and Early Islamic periods. Unfortunately, the famous Early Christian inscription from Kilwa monastery, mentioned by Bell from her 1914 visit, could not be dated by our method, because evidence indicates that it had not been continuously exposed to varnish accumulation since it its creation. Other Christian symbols associated with the early monasticism at Kilwa, which had remained exposed to the elements, yielded age estimates of *c*.1.4 ka, in close agreement with the age expected for Christian activity at the dawn of Islam in the region. Several graffiti with dates within the last 80 years gave near-zero ages, supporting our underlying assumption that surfaces with near-zero age have near-zero N_{Mn} and D_{Mn} values.

Compared with our previous sites, representations of equids are quite rare at the present sites. In our data set, they are represented by two elements showing horses with riders, both likely from the Islamic period. Armed riders reflect the tribal conflicts common in the historic period. *Wusum*, the traditional tribal symbols consisting of three characters, are widely scattered in the region, as commonly found in Arabia. The three *wusum* in our data set all suggest ages of *c*.600–800 a.

Overall, the rock art in our study area shows two distinct periods with different artistic traditions, reflecting distinct socioeconomic and ecological conditions. The hunting and herding economies in the PPN/LN are represented by a variety of game animals, human representations and symbolic elements. After a long gap with little rock art, creation follows a resurgence around the end of the Bronze Age, with rock art reflecting lifestyles adapted to arid conditions, consisting of a mixture of hunting, camel herding and trading, tribal warfare, and monastic activity. This highlights the great value of rock art for understanding human prehistory and history, especially for regions and times where other archaeological information is sparse. Our dating approach, while admittedly burdened with substantial uncertainties, provides a unique quantitative tool to assign at least rough ages to otherwise undatable rock art elements, without the need for destructive sampling.

ACKNOWLEDGMENTS

We thank the field team, including Mohammed Al-Horaish, Lazem Massoud S. Al-Sharari, Madhi Lazem Al-Sharari, Naif Lazem Mussawad Al-Sharari, Abdulillah Lazem

Al-Sharari, Mohammed A. Al-Atawi, Bata Raja Al-Harbi and Ibrahim Magbul Al-Atawi, for their valuable help during the field measurements in Saudi Arabia. We are very grateful to Ilkka Lindsted, Frédéric Imbert, Michael Macdonald and Jérôme Norris for identifying the inscriptions and providing approximate ages. We strongly appreciate the collaboration of Guillaume Charloux and the Archaeological Project of the Camel Site (supported by the CNRS and SCTH; directed by G. Charloux, M. Guagnin and A. AlSharekh) at the Camel Site. The Saudi Commission for Tourism and National Heritage is thanked for kindly giving permission to conduct the work at the field sites. This study was funded by both the Max Planck Society of Germany and the Distinguished Scientist Fellowship Program of King Saud University, Riyadh. The authors declare no conflict of interest. Open access funding enabled and organized by Projekt DEAL.

ORCID

Meinrat O. Andreae https://orcid.org/0000-0003-1968-7925
Maria Guagnin https://orcid.org/0000-0002-7995-8611
Klaus Peter Jochum https://orcid.org/0000-0002-0135-4578

REFERENCES

al-Ghazzi, A. S. (2012). The Kingdom of Midian. In A.I. Al-Ghabban, B. Andre-Salvini, F. Demange, C. Juvin & M. Cotty (Eds.), *Roads of Arabia* (pp. 211–217). Paris: Musée du Louvre.

Almushawh, M.A. (2018). An archaeoastronomical approach to the megalithic sites of Saudi Arabia. *Mediterranean Archaeology & Archaeometry*, *18*(4), 1–9. https://doi.org/10.5281/zenodo.1472244

Anati, E. (1968). *Rock Art in Central Arabia, Vol. 1: The « Oval-Headed » People of Arabia (Expédition Philby-Ryckmans-Lippens en Arabie, 1re partie: Géographie et archéologie, tome 3)*. Louvain: Université de Louvain, Institut orientaliste (Bibliothèque du Muséon, 50).

Andreae, M.O., Al-Amri, A., Andreae, T.W., Garfinkel, A., Haug, G., Jochum, K.P., … Weis, U. (2020). Geochemical studies on rock varnish and petroglyphs in the Owens and Rose Valleys, California. *PLoS ONE*, *15*. https://doi.org/10.1371/journal.pone.0235421

Aubert, M., Lebe, R., Oktaviana, A.A., Tang, M., Burhan, B, Hamrullah …Brumm, A. (2019). Earliest hunting scene in prehistoric art. *Nature*. https://doi.org/10.1038/s41586-019-1806-y

Bednarik, R.G. (2009). Experimental colorimetric analysis of petroglyphs. *Rock Art Research*, *26*(1), 55–64.

Bednarik, R.G. (2010). Developments in petroglyph dating. *Rock Art Research*, *27*(2), 217–222.

Bednarik, R.G. (2012). The use of weathering indices in rock art science and archaeology. *Rock Art Research*, *29*(1), 59–84.

Bednarik, R.G. (2013). Pleistocene palaeoart of Africa. *Arts*, *2*(1), 6–34. https://doi.org/10.3390/arts2010006

Bednarik, R.G. (2014). Pleistocene palaeoart of the Americas. *Arts*, *3*(2), 190–206. https://doi.org/10.3390/arts3020190

Bednarik, R.G. (2017). Scientific investigations into Saudi Arabian rock art: A review. *Mediterranean Archaeology and Archaeometry*, *17*, 43–59. https://doi.org/10.5281/zenodo.893192

Bednarik, R.G., & Khan, M. (2005). Scientific studies of Saudi Arabian rock art. *Rock Art Research*, *22*, 49–81.

Beherec, M.A., Levy, T.E., Tirosh, O., Najjar, M., Knabb, K.A., & Erel, Y. (2016). Iron Age nomads and their relation to copper smelting in Faynan (Jordan): Trace metal and Pb and Sr isotopic measurements from the Wadi Fidan 40 cemetery. *Journal of Archaeological Science*, *65*, 70–83. https://doi.org/10.1016/j.jas.2015.10.006

Bell, G. (1927). *The Letters of Gertrude Bell. Selected and Edited by Lady Bell, D.B.E. (Volume 1)*. New York: Boni and Liveright.

Belzoni, G. B. (Ed.) (1820). *Narrative of the operations and recent discoveries within the pyramids, temples, tombs, and excavations*. London: J. Murray.

Bergametti, G., & Forêt, G. (2014). Dust Deposition. In P. Knippertz & J.-B.W. Stuut (Eds.), *Mineral Dust: A Key Player in the Earth System* (pp. 179–200). Dordrecht: Springer.

Betts, A.V.G. (1987). The hunter's perspective: 7th millennium BC rock carvings from eastern Jordan. *World Archaeology*, *19*(2), 214–225. https://doi.org/10.1080/00438243.1987.9980035

Bishop, J.L., Murchie, S.L., Pieters, C.M., & Zent, A.P. (2002). A model for formation of dust, soil, and rock coatings on Mars: Physical and chemical processes on the Martian surface. *Journal of Geophysical Research: Planets*, *107*. https://doi.org/10.1029/2001JE001581

Bowersock, G.W. (1994). *Roman Arabia*. Cambridge, Mass.: Harvard University Press.

Broecker, W.S., & Liu, T. (2001). Rock varnish: Recorder of desert wetness? *GSA Today*, August, 4–10.

Cantrell, C.A. (2008). Review of methods for linear least-squares fitting of data and application to atmospheric chemistry problems. *Atmospheric Chemistry and Physics*, *8*, 5477–5487.

Charloux, G. (2018). Rythmes et modalités du peuplement d'une oasis du nord-ouest de l'Arabie. Sept campagnes (2010–2017) sur le site de Dûmat al-Jandal. *Comptes Rendus de l'Académie des Inscriptions et Belles-Lettres*, 11–46.

Charloux, G., al-Khalifah, H., al-Malki, T., Mensan, R., & Schwerdtner, R. (2018). The art of rock relief in ancient Arabia: new evidence from the Jawf Province. *Antiquity*, *92*, 165–182. https://doi.org/10.15184/aqy.2017.221

Charloux, G., & Loreto, R. (2011). Dûmat al-Jandal (Arabie Saoudite). Premières explorations de l'oasis antique par la mission archéologique italo-franco-saoudienne. *Comptes rendus des séances de l'Académie des Inscriptions et Belles-Lettres*, *155*(2), 905–919. https://doi.org/10.3406/crai.2011.93228

Charloux, G., & Loreto, R. (2013). *Dûmat al-Jandal. 2800 years of History in the Kingdom of Saudi Arabia*. Riyadh: Saudi Commission for Tourism and Antiquities.

Cremaschi, M. (1996). The rock varnish in the Messak Settafet (Fezzan, Libyan Sahara), age, archaeological context, and paleo-environmental implication. *Geoarchaeology*, *11*(5), 393–421.

Dinies, M., Plessen, B., Neef, R., & Kuerschner, H. (2015). When the desert was green: Grassland expansion during the early Holocene in northwestern Arabia. *Quaternary International*, *382*, 293–302. https://doi.org/10.1016/j.quaint.2015.03.007

Dorn, R.I. (2007). Rock varnish. In D.J. Nash & S.J. McLaren (Eds.), *Geochemical Sediments and Landscapes* (pp. 246–297). London: Blackwell.

Dorn, R.I. (2018). Necrogeomorphology and the life expectancy of desert bedrock landforms. *Progress in Physical Geography*, *42*(5), 566–587. https://doi.org/10.1177/0309133318795839

Dorn, R.I., & Krinsley, D. (2011). Spatial, temporal and geographic considerations of the problem of rock varnish diagenesis. *Geomorphology*, *130*, 91–99. https://doi.org/10.1016/j.geomorph.2011.02.002

Dorn, R.I., Krinsley, D.H., Langworthy, K.A., Ditto, J., & Thompson, T.J. (2013). The influence of mineral detritus on rock varnish

formation. *Aeolian Research*, *10*, 61–76. https://doi.org/10.1016/j.aeolia.2013.04.005

Dragovich, D. (2000). Rock engraving chronologies and accelerator mass spectrometry radiocarbon age of desert varnish. *Journal of Archaeological Science*, *27*(10), 871–876. https://doi.org/10.1006/jasc/1999.0586

Drechsler, P. (2007). The Neolithic dispersal into Arabia. *Proceedings of the Seminar for Arabian Studies*, *37*, 93–109.

Engel, C.G., & Sharp, R.P. (1958). Chemical data on desert varnish. *Geological Society of America Bulletin*, *69*(5), 487–518. https://doi.org/10.1130/0016-7606(1958)69[487:cdodv]2.0.co;2

Engel, M., Brueckner, H., Pint, A., Wellbrock, K., Ginau, A., Voss, P., … Frenzel, P. (2012). The early Holocene humid period in NW Saudi Arabia—Sediments, microfossils and palaeo-hydrological modelling. *Quaternary International*, *266*, 131–141. https://doi.org/10.1016/j.quaint.2011.04.028

Farès, S. (2010). L'inscription arabe de Kilwa: nouvelle lecture. *Semitica et Classica*, *3*, 241–248. https://doi.org/10.1484/J.SEC.1.100941

Farès, S. (2011). Christian monasticism on the eve of Islam: Kilwa (Saudi Arabia)—new evidence. *Arabian Archaeology and Epigraphy*, *22*(2), 243–252. https://doi.org/10.1111/j.1600-0471.2011.00335.x

Francis, J., & Loendorf, L.L. (2004). *Ancient Visions—Petroglyphs and Pictographs of the Wind River and Bighorn Country, Wyoming and Montana*. Salt Lake City, Utah: University of Utah Press.

Francis, J.E., Loendorf, L.L., & Dorn, R.I. (1993). AMS radiocarbon and cation-ratio dating of rock art in the Bighorn Basin of Wyoming and Montana. *American Antiquity*, *58*(4), 711–737. https://doi.org/10.2307/282204

Fujii, S. (2013). Chronology of the Jafr prehistory and protohistory: A key to the process of pastoral nomadization in the Southern Levant. *Syria*, *90*, 49–125.

Garfinkel, A.P., Young, D.A., & Yohe, R.M. (2010). Bighorn hunting, resource depression, and rock art in the Coso Range, eastern California: a computer simulation model. *Journal of Archaeological Science*, *37*(1), 42–51. https://doi.org/10.1016/j.jas.2009.08.010

Garrard, A., & Harvey, C.P.D. (1977). Environment and settlement during the upper Pleistocene and Holocene at Jubbah in the Great Nafud, North Arabia. *Atlal J. Saudi Arab. Archaeology*, *5*, 137–156.

Gebel, H.G.K. (2016). The socio-hydraulic foundations of oasis life in NW Arabia: The 5th Millennium BCE shepherd environs of Rajajil, Rasif and Qulban Beni Murra. In M. Luciani (Ed.), *The Archaeology of North Arabia—Oases and Landscapes* (pp. 79–114). Vienna: Austrian Academy of Sciences.

Gilmore, M., Al-Ibrahim, M., & Murad, A.S. (1982). Preliminary Report on the Northwestern and Northern Region Survey 1981 (1401). *Atlal J. Saudi Arab. Archaeology*, *6*, 9–23.

Goldsmith, Y. (2011). *Characterizing rock varnish developed on earliest Holocene Negev flint artifacts as a potential paleoenvironmental or paleoclimatic indicator*. Jerusalem: Geological Survey of Israel.

Goldsmith, Y., Stein, M., & Enzel, Y. (2014). From dust to varnish: Geochemical constraints on rock varnish formation in the Negev Desert, Israel. *Geochimica et Cosmochimica Acta*, *126*, 97–111. https://doi.org/10.1016/j.gca.2013.10.040

Grattan, J.P., Adams, R.B., Friedman, H., Gilbertson, D.D., Haylock, K.I., Hunt, C.O., & Kent, M. (2016). The first polluted river? Repeated copper contamination of fluvial sediments associated with Late Neolithic human activity in southern Jordan. *Science of the Total Environment*, *573*, 247–257. https://doi.org/10.1016/j.scitotenv.2016.08.106

Guagnin, M., Jennings, R., Eager, H., Parton, A., Stimpson, C., Stepanek, C., … Petraglia, M.D. (2016). Rock art imagery as a proxy for Holocene environmental change: A view from Shuwaymis, NW Saudi Arabia. *Holocene*, *26*(11), 1822–1834. https://doi.org/10.1177/0959683616645949

Guagnin, M., Jennings, R.P., Clark-Balzan, L., Groucutt, H.S., Parton, A., & Petraglia, M.D. (2015). Hunters and herders: Exploring the Neolithic transition in the rock art of Shuwaymis, Saudi Arabia. *Archaeological Research in Asia*, *4*, 3–16. https://doi.org/10.1016/j.ara.2015.08.001

Guagnin, M., Perri, A.R., & Petraglia, M.D. (2018a). Pre-Neolithic evidence for dog-assisted hunting strategies in Arabia. *Journal of Anthropological Archaeology*, *49*, 225–236. https://doi.org/10.1016/j.jaa.2017.10.003

Guagnin, M., Shipton, C., al-Rashid, M., Moussa, F., El-Dossary, S., Sleimah, M. B., …Petraglia, M. (2017). An illustrated prehistory of the Jubbah oasis: Reconstructing Holocene occupation patterns in north-western Saudi Arabia from rock art and inscriptions. *Arabian Archaeology and Epigraphy*, *28*(2), 138–152. https://doi.org/10.1111/aae.12089

Guagnin, M., Shipton, C., el-Dossary, S., al-Rashid, M., Moussa, F., Stewart, M., … Petraglia, M. D. (2018b). Rock art provides new evidence on the biogeography of kudu (*Tragelaphus imberbis*), wild dromedary, aurochs (*Bos primigenius*), and African wild ass (*Equus africanus*) in the early and middle Holocene of north-western Arabia. *Journal of Biogeography*, *45*, 727–740. https://doi.org/10.1111/jbi.13165

Harding, G.L., & Littmann, E. (1952). *Some Thamudic Inscriptions from the Hashemite Kingdom of Jordan*. Leiden: Brill.

Hashim, S.A. (1996). Typology, evolutions and developments of funerary structures in Saudi Arabian antiquities. *Atlal*, *14*, 102–128.

Hauptmann, A. (2007). *The Archaeometallurgy of Copper—Evidence from Faynan, Jordan*. New York: Springer.

Heizer, R.F., & Baumhoff, M.A. (1962). *Prehistoric Rock Art of Nevada and Eastern California*. Berkeley and Los Angeles, California: University of California Press.

Horsfield, A. (1943). Journey to Kilwa, Transjordan. *The Geographical Journal*, *102*(2), 71–77. https://doi.org/10.2307/1790135

Horsfield, G., Horsfield, A., & Glueck, N. (1933). Prehistoric Rock-Drawings in Transjordan. *American Journal of Archaeology*, *37*(3), 381–386. https://doi.org/10.2307/498950

Hoyland, R.G. (2001). *Arabia and the Arabs—From the Bronze Age to the coming of Islam*. London: Routledge.

Hoyland, R.G. (2017). Two new Arabic inscriptions: Arabian castles and Christianity in the Umayyad period. In L. Nehmé & A. Al-Jallad (Eds.), *To the Madbar and back again: Studies in the languages, archaeology, and cultures of Arabia dedicated to Michael C. A. Macdonald* (pp. 327–338). Leiden: Brill.

Huyge, D., Vandenberghe, D.A.G., De Dapper, M., Mees, F., Claes, W., & Darnell, J.C. (2011). First evidence of Pleistocene rock art in North Africa: securing the age of the Qurta petroglyphs (Egypt) through OSL dating. *Antiquity*, *85*(330), 1184–1193. https://doi.org/10.1017/s0003598x00061998

Ingraham, M.L., Johnson, T.D., Rihani, B., & Shatla, I. (1981). Preliminary Report on a Reconnaissance Survey of the Northwestern Province (With a Note on a Brief Survey of the Northern Province). *Atlal J. Saudi Arab. Archaeology*, *5*, 59–83.

Jickells, T.D., An, Z.S., Andersen, K.K., Baker, A.R., Bergametti, G., Brooks, N., … Torres, R. (2005). Global iron connections

between desert dust, ocean biogeochemistry, and climate. *Science*, *308*(5718), 67–71.

Jochum, K.P., Nohl, L., Herwig, K., Lammel, E., Stoll, B., & Hofmann, A.W. (2005). GeoReM: A new geochemical database for reference materials and isotopic standards. *Geostandards and Geoanalytical Research*, *29*(3), 333–338. https://doi.org/10.1111/j.1751-908X.2005.tb00904.x

Khan, M. (2007). *The Rock Art of Saudi Arabia Across Twelve Thousand Years*. Riyadh, Saudi Arabia: Deputy Ministry of Antiquities & Museums.

Khan, M. (2013). *Rock Art of Saudi Arabia. Arts*, *2*, 447–475. https://doi.org/10.3390/arts2040447

Khan, M. (2017). *The Rock Art of Saudi Arabia*. Riyadh: Saudi Commission for Tourism and National Heritage.

Klasen, N., Engel, M., Brueckner, H., Hausleiter, A., Intilia, A., Eichmann, R., … al-Said, S. F., (2011). Optically stimulated luminescence dating of the city wall system of ancient Tayma (NW Saudi Arabia). *Journal of Archaeological Science*, *38*(8), 1818–1826. https://doi.org/10.1016/j.jas.2011.03.018

Krinsley, D., Ditto, J., Langworthy, K., Dorn, R.I., & Thompson, T. (2013). Varnish microlaminations: new insights from focused ion beam preparation. *Physical Geography*, *34*, 159–173. https://doi.org/10.1080/02723646.2013.830926

Lebedeva, M.P., Golovanov, D.L., Shishkov, V.A., Ivanov, A.L., & Abrosimov, K.N. (2019). Microscopic and tomographic studies for interpreting the genesis of desert varnish and the vesicular horizon of desert soils in Mongolia and the USA. *Boletin de la Sociedad Geologica Mexicana*, *71*(1), 21–42. https://doi.org/10.18268/BSGM2019v71n1a3

Lezine, A.-M., Tiercelin, J.-J., Robert, C., Saliege, J.-F., Cleuziou, S., Inizan, M.-L., & Braemer, F. (2007). Centennial to millennial-scale variability of the Indian monsoon during the early Holocene from a sediment, pollen and isotope record from the desert of Yemen. *Palaeogeography Palaeoclimatology Palaeoecology*, *243*(3–4), 235–249. https://doi.org/10.1016/j.palaeo.2006.05.019

Liu, T., & Broecker, W.S. (2007). Holocene rock varnish microstratigraphy and its chronometric application in the drylands of western USA. *Geomorphology*, *84*(1–2), 1–21. https://doi.org/10.1016/j.geomorph.2006.06.008

Liu, T.H., & Broecker, W.S. (2000). How fast does rock varnish grow? *Geology*, *28*(2), 183–186.

Liu, T.Z., & Broecker, W.S. (2008). Rock varnish evidence for latest Pleistocene millennial-scale wet events in the drylands of western United States. *Geology*, *36*(5), 403–406. https://doi.org/10.1130/g24573a.1

Liu, T.Z., & Broecker, W.S. (2013). Millennial-scale varnish microlamination dating of late Pleistocene geomorphic features in the drylands of western USA. *Geomorphology*, *187*, 38–60. https://doi.org/10.1016/j.geomorph.2012.12.034

Liu, T.Z., Broecker, W.S., Bell, J.W., & Mandeville, C.W. (2000). Terminal Pleistocene wet event recorded in rock varnish from Las Vegas Valley, southern Nevada. *Palaeogeography Palaeoclimatology Palaeoecology*, *161*, 423–433. https://doi.org/10.1016/s0031-0182(00)00097-3

lnizan, M.-L. (2012). The Prehistoric Populations. In A.I. Al-Ghabban, B. Andre-Salvini, F. Demange, C. Juvin & M. Cotty (Eds.), *Roads of Arabia* (pp. 138–157). Paris: Musée du Louvre.

Loreto, R., & Charloux, G. (2013). The Saudi–Italian–French Archaeological Project at Dûmat al-Jandal (Preliminary Report of the 2012 Season). *Newsletter di Archeologia CISA*, *4*, 211–251.

Lytle, F., Lytle, M., Rogers, A., Garfinkel, A., Maddock, C., Wight, W., & Cole, C. (2008). *An experimental technique for measuring age of petroglyph production: results on Coso petroglyphs (available at: https://www.academia.edu/4539728/An_Experimental_Technique_for_Measuring_Age_of_Petroglyph_Production_Results_on_Coso_Petroglyphs)*. Paper presented at the Great Basin Anthropological Conference, Portland, OR.

Macdonald, M.C.A. (2000). Reflections on the linguistic map of pre-Islamic Arabia. *Arabian Archaeology and Epigraphy*, *11*, 28–79.

Macdonald, M.C.A. (2004). Ancient North Arabian. In R.D. Woodard (Ed.), *The Cambridge Encyclopedia of the World's Ancient Languages* (pp. 488–533). Cambridge: Cambridge University Press.

Macdonald, M.C.A. (2010). Ancient Arabia and the written word. In M.C.A. Macdonald (Ed.), *The development of Arabic as a written language*. (Supplement to the Proceedings of the Seminar for Arabian Studies 40) (pp. 5–28). Oxford: Archaeopress.

Macholdt, D.S., Al-Amri, A.M., Tuffaha, H.T., Jochum, K.P., & Andreae, M.O. (2018). Growth of desert varnish on petroglyphs from Jubbah and Shuwaymis, Ha'il region, Saudi Arabia. *The Holocene*, *28*(9), 1495–1511. https://doi.org/10.1177/0959683618777075

Macholdt, D.S., Herrmann, S., Jochum, K.P., Kilcoyne, A.L.D., Laubscher, T., Pfisterer, J.H.K., … Andreae, M.O. (2017a). Black manganese-rich crusts on a Gothic cathedral. *Atmospheric Environment*, *171*, 205–220. https://doi.org/10.1016/j.atmosenv.2017.10.022

Macholdt, D.S., Jochum, K.P., Al-Amri, A., & Andreae, M.O. (2019). Rock varnish on petroglyphs from the Hima region, southwestern Saudi Arabia: Chemical composition, growth rates, and tentative ages. *The Holocene*, *29*, 1377–1395. https://doi.org/10.1177/0959683619846979

Macholdt, D.S., Jochum, K.P., Pöhlker, C., Arangio, A., Förster, J.D., Stoll, B., … Andreae, M.O. (2017b). Characterization and differentiation of rock varnish types from different environments by microanalytical techniques. *Chemical Geology*, *459*, 91–118. https://doi.org/10.1016/j.chemgeo.2017.04.009

Magee, P. (2014a). *The Archaeology of Prehistoric Arabia: Adaptation and Social Formation from the Neolithic to the Iron Age*. Cambridge: Cambridge University Press.

Magee, P. (2014b). The Formation of Arabian Society: 7000–3000 BC. In P. Magee (Ed.), *The Archaeology of Prehistoric Arabia: Adaptation and Social Formation from the Neolithic to the Iron Age* (pp. 46–86). Cambridge: Cambridge University Press.

McClure, H.A. (1976). Radiocarbon chronology of late quaternary lakes in the Arabian desert. *Nature*, *263*(5580), 755–756. https://doi.org/10.1038/263755a0

McCorriston, J., & Martin, L. (2010). Southern Arabia's Early Pastoral Population History: Some Recent Evidence. In M.D. Petraglia & J.I. Rose (Eds.), *The Evolution of Human Populations in Arabia: Paleoenvironments, Prehistory and Genetics* (pp. 237–250). Dordrecht: Springer, Netherlands.

McNeil, J. (2010). Making Lemonade. Using Graffiti to Date Petroglyphs. *Utah Rock Art*, 9–21.

Munro, N.D., Bar-Oz, G., Meier, J.S., Sapir-Hen, L., Stiner, M.C., & Yeshurun, R. (2018). The emergence of animal management in the Southern Levant. *Scientific Reports*, *8*(1), https://doi.org/10.1038/s41598-018-27647-z

Nehmé, L. (2017). New dated inscriptions (Nabataean and pre-Islamic Arabic) from a site near al-Jawf, ancient Dūmah, Saudi Arabia. *Arabian Epigraphic Notes*, *3*, 121–164.

Nehmé, L., Al-Talhi, D., & Villeneuve, F. (2012). Hegra of Arabia Felix. In A.I. Al-Ghabban, B. Andre-Salvini, F. Demange, C. Juvin & M. Cotty (Eds.), *Roads of Arabia*. Paris: Musée du Louvre.

Nehmé, L., al-Talhi, D., & Villeneuve, F. (2014). *Report on the Third Excavation Season (2010) of the Madâ'in Sâlih Archaeological Project*. Riyadh.

Nehmé, L., Arnoux, T., Bessac, J.C., Braun, J.P., Dentzer, J.M., Kermorvant, A., … Rigot, J.B. (2006). Mission archéologique de Mada'in Salih (Arabie Saoudite): Recherches menées de 2001 à 2003 dans l'ancienne Hijra des Nabatéens (1). *Arabian Archaeology and Epigraphy*, *17*(1), 41–124. https://doi.org/10.1111/j.1600-0471.2006.00249.x

Newton, L.S., & Zarins, J. (2000). Aspects of Bronze Age art of southern Arabia: The pictorial landscape and its relation to economic and scoio-political status. *Arabian Archaeology and Epigraphy*, *11*(2), 154–179. https://doi.org/10.1111/j.1600-0471.2000.aae110202.x

Norris, J. (2018). A survey of the Ancient North Arabian inscriptions from the Dūmat al-Jandal area (Saudi Arabia). In M.C.A. Macdonald (Ed.), *Languages, scripts and their uses in ancient North Arabia*. (Supplement to volume 48 of the Proceedings of the Seminar for Arabian Studies) (pp. 71–93). Oxford: Archaeopress.

Olsen, S.L. (2013). *Stories in the rocks: exploring Saudi Arabian rock art*. Carnegie Museum of Natural History.

Otter, L.M., Macholdt, D.S., Jochum, K.P., Stoll, B., Weis, U., Weber, B., … Andreae, M.O. (2020). Geochemical insights into the relationship of rock varnish and adjacent mineral dust fractions. *Chemical Geology*, *551*. https://doi.org/10.1016/j.chemgeo.2020.119775

Parker, A. (2010). Pleistocene Climate Change in Arabia: Developing a Framework for Hominin Dispersal over the Last 350 ka. In M.D. Petraglia & J.I. Rose (Eds.), *The Evolution of Human Populations in Arabia, Vertebrate Paleobiology and Paleoanthropology* (pp. 39–49). Springer.

Perry, R.S., Kolb, V.M., Lynne, B.Y., Sephton, M.A., McLoughlin, N., Engel, M.H., Staley, J.T. (2005). How desert varnish forms? *Proceedings of the SPIE—The International Society for Optical Engineering*, *5906*, 276–287. https://doi.org/10.1117/12.626547

Petraglia, M.D. (2003). The Lower Paleolithic of the Arabian Peninsula: Occupations, adaptations, and dispersals. *Journal of World Prehistory*, *17*(2), 141–179.

Pike, A.W.G., Hoffmann, D.L., Garcia-Diez, M., Pettitt, P.B., Alcolea, J., De Balbin, R., … Zilhao, J. (2012). U-series dating of Paleolithic art in 11 caves in Spain. *Science*, *336*(6087), 1409–1413. https://doi.org/10.1126/science.1219957

Potter, R.M., & Rossman, G.R. (1977). Desert varnish—Importance of clay minerals. *Science*, *196*(4297), 1446–1448. https://doi.org/10.1126/science.196.4297.1446

Potter, R.M., & Rossman, G.R. (1979). The manganese- and iron-oxide mineralogy of desert varnish. *Chemical Geology*, *25*, 79–94.

Potts, D.T. (2012). The story of the origins. In A.I. Al-Ghabban, B. Andre-Salvini, F. Demange, C. Juvin & M. Cotty (Eds.), *Roads of Arabia* (pp. 71–78). Paris: Musée du Louvre.

Ramanaidou, E.R., & Fonteneau, L.C. (2019). Rocky relationships: the petroglyphs of the Murujuga (Burrup Peninsula and Dampier Archipelago) in Western Australia. *Australian Journal of Earth Sciences*, *66*(5), 671–698. https://doi.org/10.1080/08120099.2019.1577299

Reneau, S.L. (1993). Manganese accumulation in rock-varnish on a desert piedmont, Mojave Desert, California, and application to evaluating varnish development. *Quaternary Research*, *40*(3), 309–317. https://doi.org/10.1006/qres.1993.1084.

Rhotert, H., Böhl, F.M.T., & Willmann, K. (1938). *Transjordanien—Vorgeschichtliche Forschungen* (A. E. Jensen & H. Rhotert (Eds.) Verlauf und Ergebnisse der XII. Deutschen Inner-Afrikanischen Forschungs-Expedition (DIAFE) 1934/35: Vorgeschichtliche Forschungen in Kleinasien und Nordafrika). Stuttgart: Strecker und Schröder.

Robin, C. (2018). La faune de l'arabie heureuse: Les textes et les images rupestres de Ḥimà. In J. Jouanna, C. Robin & M. Zinc (Eds.), *Actes, Colloque « Vie et climat d'Hésiode à Montesquieu », Cahiers de la villa « Kérylos », 29, Beaulieu-sur-mer, Alpes maritimes* (pp. 319–384). Paris: Diffusion de Boccard.

Robin, C.J., & Al-Ghabbān, A.I. (2017). Une première mention de Madyan dans un texte épigraphique d'Arabie. *Comptes rendus des séances de l'Académie des Inscriptions et Belles-Lettres*, *I*, 363–396.

Robin, C.J., & Gorea, M. (2016). L'alphabet de Ḥimà (Arabie séoudite). In C. J. R. T. R. Israel Finkelstein (Ed.), *Alphabets, Texts and Artefacts in the Ancient Near East: Studies Presented to Benjamin Sass* (pp. 312–377). Paris: Van Dieren.

Rogers, A.K. (2010). A chronology of six rock art motifs in the Coso Range, Eastern California. *American Indian Rock Art*, *36*, 23–36.

Rudnick, R.L., & Gao, S. (2003). 3.01—Composition of the Continental Crust. In H.D. Holland & K.K. Turekian (Eds.), *Treatise on Geochemistry* (pp. 1–64). Oxford: Pergamon.

Soukopova, J. (2018). Decorated boulders and other neglected features of the Central Saharan rock art. *Journal of Arid Environments*, *156*, 96–105. https://doi.org/10.1016/j.jaridenv.2018.05.001

Sowers, J.M. (2013). Rock varnish chronometry: Methods and Applications. In J.S. Noller, J.M. Sowers & W.R. Lettis (Eds.), *Quaternary Geochronology* (pp. 241–260). Washington, DC: American Geophysical Union.

Stein, P. (2013). Palaeography of the Ancient South Arabian script. New evidence for an absolute chronology. *Arabian Archaeology and Epigraphy*, *24*(2), 186–195. https://doi.org/10.1111/aae.12024

Sudarchikova, N., Mikolajewicz, U., Timmreck, C., O'Donnell, D., Schurgers, G., Sein, D., & Zhang, K. (2015). Modelling of mineral dust for interglacial and glacial climate conditions with a focus on Antarctica. *Clim. Past*, *11*, 765–779. https://doi.org/10.5194/cp-11-765-2015

Tang, H., Kumar, G., Anni, J., Wu, J., Liu, W., & Bednarik, R.G. (2018). The 2015 rock art missions in China. *Rock Art Research*, *35*(1), 25–34.

Thiagarajan, N., & Lee, C.T.A. (2004). Trace-element evidence for the origin of desert varnish by direct aqueous atmospheric deposition. *Earth and Planetary Science Letters*, *224*(1–2), 131–141. https://doi.org/10.1016/j.espl.2004.04.038

Uerpmann, H.-P., Potts, D.T., & Uerpmann, M. (2010). Holocene (Re-) Occupation of Eastern Arabia. In M.D. Petraglia & J.I. Rose (Eds.), *The Evolution of Human Populations in Arabia: Paleoenvironments, Prehistory and Genetics* (pp. 205–214). Dordrecht: Springer, Netherlands.

Uerpmann, M. (2002). The Dark Millennium—remarks on the final Stone Age in the Emirates and Oman. In D. Potts & H. al-Naboodah, & P. Hellyer, (Eds.), *Archaeology of the United Arab Emirates. Proceedings of the First International Conference on the Archaeology of the U.A.E.* (pp. 74–81). London: Trident Press.

Uerpmann, M., & Uerpmann, H. (2012). Archeozoology of camels in South-Eastern Arabia. In E. Knoll & P. Burger (Eds.), *Camels in Asia and North Africa. Interdisciplinary Perspectives on Their*

Significance in Past and Present (pp. 109–122). Vienna: Academy of Sciences Press.

Watchman, A. (2000). A review of the history of dating rock varnishes. *Earth-Science Reviews*, *49*(1–4), 261–277. https://doi.org/10.1016/S0012-8252(99)00059-8

Wayne, D.M., Diaz, T.A., Fairhurst, R.J., Orndorff, R.L., & Pete, D.V. (2006). Direct major- and trace-element analyses of rock varnish by high resolution laser ablation inductively-coupled plasma mass spectrometry (LA-ICPMS). *Applied Geochemistry*, *21*(8), 1410–1431. https://doi.org/10.1016/j.apgeochem.2006.04.005

Wenning, R. (2007). The Nabataeans in History. In K.D. Politis (Ed.), *The World of the Nabataeans* (pp. 25–44). Stuttgart: Franz Steiner Verlag.

Whitley, D.S. (2012). In Suspect Terrain: Dating Rock Engravings. In J. McDonald & P. Veth (Eds.), *A Companion to Rock Art* (pp. 605–624). Blackwell.

Whitley, D.S. (2013). Rock art dating and the peopling of the Americas. *Journal of Archaeology*, 15 p. https://doi.org/10.1155/2013/713159

Whitley, D.S., & Dorn, R.I. (2007). The Coso petroglyph chronology. *Pacific Coast Archaeological Society Quarterly*, *43*, 135–157.

Whitley, D.S., Santoro, C.M., & Valenzuela, D. (2017). Climate change, rock coatings, and the archaeological record. *Elements*, *13*(3), 183–186. https://doi.org/10.2113/gselements.13.3.183

Xu, X., Li, Y., Li, Y., Lu, A., Qiao, R., Liu, K., … Wang, C. (2019). Characteristics of desert varnish from nanometer to micrometer scale: A photo-oxidation model on its formation. *Chemical Geology*, *522*, 55–70. https://doi.org/10.1016/j.chemgeo.2019.05.016

Zarins, J. (1979). Rajajil—A Unique Arabian Site from the Fourth Millennium B.C. *Atlal J. Saudi Arab. Archaeology*, *3*, 73–77.

Zarins, J. (1990). Early pastoral nomadism and the settlement of Lower Mesopotamia. *Bulletin of the American Schools of Oriental Research*, *280*, 31–65. https://doi.org/10.2307/1357309

Zerboni, A. (2008). Holocene rock varnish on the Messak plateau (Libyan Sahara): Chronology of weathering processes. *Geomorphology*, *102*(3), 640–651. https://doi.org/10.1016/j.geomorph.2008.06.010

Zerboni, A., Esposti, M.D., Wu, Y.-L., Brandolini, F., Mariani, G.S., Villa, F., … Cremaschi, M. (2019). Age, palaeoenvironment, and preservation of prehistoric petroglyphs on a boulder in the oasis of Salut (northern Sultanate of Oman). *Quaternary International*. https://doi.org/10.1016/j.quaint.2019.06.040

SUPPORTING INFORMATION

Additional supporting information may be found online in the Supporting Information section.

How to cite this article: Andreae MO, Al-Amri A, Andreae CM, et al. Archaeometric studies on the petroglyphs and rock varnish at Kilwa and Sakaka, northern Saudi Arabia. *Arab Arch Epig*. 2020;00:1–26. https://doi.org/10.1111/aae.12167